

---

## Calorimetric study of carbon dioxide (CO<sub>2</sub>) hydrate formation and dissociation processes in porous media

Benmesbah Fatima Doria <sup>1, 2, \*</sup>, Clainv Pascal <sup>1, 3, \*</sup>, Fandino Olivia <sup>2</sup>, Osswald Veronique <sup>1</sup>, Fournaison Laurence <sup>1</sup>, Dicharry Christophe <sup>4</sup>, Ruffine Livio <sup>2</sup>, Delahaye Anthony <sup>1</sup>

<sup>1</sup> Université Paris-Saclay, INRAE, FRISE, 92761, Antony, France

<sup>2</sup> Geo-Ocean, Univ Brest, CNRS, Ifremer, UMR6538, F-29280 Plouzane, France

<sup>3</sup> Leonard de Vinci Pôle Universitaire, Research Center, 12 avenue Léonard de Vinci, 92916, Paris La Défense, France

<sup>4</sup> CNRS/TOTALENERGIES/UNIV PAU & PAYS ADOUR, Laboratoire des Fluides Complexes et leurs Réservoirs - IPRA, UMR5150, 64000, Pau, France

\* Corresponding authors : Fatima Doria Benmesbah, email address :

[benmesbah.fatimadoria@gmail.com](mailto:benmesbah.fatimadoria@gmail.com) ; Pascal Clainv, email address : [pascal.clain@devinci.fr](mailto:pascal.clain@devinci.fr)

---

### Abstract :

Understanding the formation and dissociation mechanisms of gas hydrate in porous media is important for the development of new energy-efficient and environmentally friendly technologies related to cold storage as they provide significant latent heat and energy density at suitable phase change temperature. The challenge is to understand the interactions between gas hydrates and the chosen storage media in order to assess the operating conditions likely to optimize time and energy consumption in cold production and storage systems. In this work, CO<sub>2</sub> hydrates formation and dissociation are investigated in two morphologically different porous materials: sand and silica gels. A calorimetric approach is applied to study both the CO<sub>2</sub> hydrate formation kinetics, particularly the induction time, and the amount of hydrate formed for each of the two porous materials. The experiments are performed using a differential thermal analysis device with two identical measuring cells. The present work is focused on assessing the effect of key factors like water saturation, particle size and the morphology of porous media on CO<sub>2</sub> hydrate formation and dissociation processes. Overall, the results do not show a statistically significant correlation between these factors and the induction time. Interestingly, the results obtained with dual porous silica gel showed a higher amount of hydrate formed compared to those with sand for similar initial pressure, temperature and water content conditions. This result may be due to the fact that silica gels provide higher surface area due to their smaller particle size (20-45 µm vs. 80-450 µm for sand), and the presence of internal pore volume in silica gel particles.

---

## Highlights

► Calorimetric study of CO<sub>2</sub> hydrates formation and dissociation in silica sand and gel. ► Induction time of CO<sub>2</sub> hydrates is not influenced by water saturation. ► Silica sand of particle size of have a great effect on the amount of hydrates formed. ► Morphology of porous medium used have a big impact on the amount of hydrates formed. ► Better results have been obtained with silica gel than Fontainebleau sand.

**Keywords** : CO<sub>2</sub> hydrate, Cold storage, Differential thermal analysis, Particle and Pore size, Porous media, Water saturation

## 36 **1. Introduction**

37 Industry requirements for thermal energy production and storage are increasing to meet human  
38 needs, for example, for food conservation, refrigeration and air conditioning. However, cold  
39 production is responsible for 20 % of the electrical energy consumed in industrial countries and  
40 8 % of greenhouse gas emissions due to traditional refrigeration processes. Indeed, these  
41 processes use harmful refrigerants such as Chlorofluorocarbons (CFCs) and  
42 Hydrochlorofluorocarbons (HCFCs) that are relevant to radiative forcing and stratospheric  
43 ozone depletion, but also, Hydrofluorocarbons (HFCs) which, like CO<sub>2</sub>, are linked only to  
44 radiative forcing. These coolants have a much higher global warming potential than carbon  
45 dioxide (for example, CFC-12, HCFC-22 and HFC-134a are respectively 10 900, 1 810 and  
46 1 430 times as warming as carbon dioxide over a 100-year period (Forster and Venkatachalam,  
47 2005). In an attempt to contain and reduce the use of these refrigerants, secondary refrigeration  
48 has been proposed as an interesting and promising solution. It introduces the use of  
49 environmentally neutral refrigerants that conduct thermal energy in a secondary circuit to the  
50 cooling point (Delahaye et al., 2018; Wang et al., 2015).

51 The development of a cost-effective and environmentally friendly secondary refrigeration  
52 system requires a good balance between energy demand and supply. In this context, the cooling  
53 capacity of the system has to be sufficient during peak hours when energy consumption is high.  
54 Cold storage is a suitable method to increase this cooling capacity. Indeed, cold storage devices  
55 can be used to store cold thermal energy during off-peak periods, and use it during peak hours,  
56 which contributes to peak shaving and refrigerating system downsizing. Hence, cold storage  
57 offers flexibility in energy consumption by ensuring spatial and temporal regulation. This is  
58 why most of the industrial achievements combine cold production and storage systems.  
59 Traditionally, cold storage technologies use ice, chilled water or eutectic salt (Akbari and  
60 Mertol, 1989; Cheng et al., 2020). However, some of these storage media have low energy  
61 efficiency and can be very costly (Hasnain, 1998). The challenge of this technology is to select

62 a refrigerant with high energy density and high heat transfer capacity in order to reduce the  
63 system power consumption. One of the solutions that is currently under consideration is the use  
64 of phase change materials for such a technology.

65 Among the phase change materials that have the most suitable criteria for the refrigeration  
66 industry, gas hydrates have attracted the attention of several researchers who considered them  
67 as a potential candidate, primarily due to their interesting thermodynamic properties (Sloan,  
68 1998; Sloan and Fleyfel, 1992). Gas hydrates are non-stoichiometric crystalline structures  
69 composed of hydrogen-bonded water molecules forming cavities, generally called cages. These  
70 cavities can trap gas molecules like hydrogen, nitrogen, helium, methane, carbon dioxide or  
71 hydrocarbons and so on (Loveday and Nelmes, 2008; Sloan and Koh, 2007), which stabilizes  
72 the hydrate structure. Gas hydrates are stable under low temperature and high-pressure  
73 conditions. The attractive properties of gas hydrates include their high gas storage capacity,  
74 their increased gas selectiveness capacity and their high dissociation enthalpy. In addition, they  
75 are stable over a wide range of temperatures (in particular for  $T > 273$  K, for example,  $\text{CO}_2$   
76 hydrates can form at a rough range of temperatures between 273 and 283 K, and an approximate  
77 pressure range of 1.5-4.5 MPa), which is of a particular interest for air conditioning (Englezos,  
78 1993; Fournaison et al., 2004; Li et al., 2012).

79 The development of a  $\text{CO}_2$  hydrate-based cold production, transport and storage system requires  
80 intensive studies on the kinetic, thermodynamic and rheological characteristics of  $\text{CO}_2$  hydrate  
81 slurries (gas hydrate crystals suspended in water), which were the focuses of many studies in  
82 the past (Boufares et al., 2018; Darbouret et al., 2005; Delahaye et al., 2008; Dufour et al., 2017;  
83 Jerbi et al., 2010; Kumar et al., 2016; Prah and Yun, 2018; Shindo et al., 1993). Several of them  
84 pointed out a slow gas hydrate formation rate and a low storage density in bulk media (Englezos  
85 et al., 1987; Linga et al., 2010). In order to enhance energy efficiency of hydrate-based  
86 industrial applications, several solutions that involve specific properties have been proposed

87 such as **acceleration of the formation process by stirring in order** to improve **gas mass** transfer  
88 **to liquid** by enhancing the **gas-liquid contact** interface (Linga et al., 2012; Wang et al., 2014);  
89 the use of acoustic waves (Laugier et al., 2008; Wang and Dennis, 2017) or the use of kinetic  
90 or thermodynamic chemical additives (Joshi et al., 2013; Kang et al., 2001; Kumar et al., 2013;  
91 Martínez et al., 2008; Torr  et al., 2011). According to a recent review of literature enhancing  
92 mass transfer by forming CO<sub>2</sub> hydrates in porous media could improve Cold Thermal Energy  
93 Storage (CTES) design (Wang et al., 2020). However, related current research is focused on  
94 other applications such as gas separation (Yang et al., 2015), CO<sub>2</sub> sequestration (Oya et al.,  
95 2017), and mainly on understanding natural hydrate dynamics (Malagar et al., 2019; Zhang et  
96 al., 2017). To our knowledge, very few studies have been published on the use of porous media  
97 in CO<sub>2</sub> hydrate-based cold storage technologies. Indeed Clain (2014) mentioned the interest  
98 and the kinetic and thermodynamic influence of porous media which can constitute a simple  
99 solution to implement for the development of a multi-temperature storage process from  
100 hydrates. More recently, Cheng et al. (2020) reported on the use of porous media as a hydrate  
101 reinforcement method aiming at reducing the induction time of hydrate formation, increasing  
102 nucleation rates, and bettering the cold storage density of the cold storage media. In addition,  
103 as mentioned previously Wang et al. (2020) pointed out in a review that one of the important  
104 challenges of CTES systems based on CO<sub>2</sub> hydrates is a low mass transfer due to limited gas-  
105 liquid interface. The authors suggested the use of porous media in future work to improve mass  
106 transfer and thus the gas-liquid interface.

107 In a series of investigation on gas hydrates formation and dissociation kinetics, **it has been**  
108 shown an improvement of gas hydrate formation as well as water to hydrate conversion rates  
109 in a packed bed of silica sand particles compared to a stirred vessel (bulk media) (Linga and  
110 Clarke, 2017; Linga et al., 2009). Indeed, porous media offer a relatively large contact surface  
111 compared to bulk media. They allow a better distribution of the liquid and vapor phases by

112 adsorption on the surface of the particles and with the help of capillary forces, thus increasing  
113 the gas-water contact. Therefore, the mechanisms of gas hydrate formation and dissociation in  
114 porous media must be carefully considered.

115 In order to provide a large surface area and potentially to limit energy consumption related to  
116 the stirring required in bulk media, the present paper seeks to address CO<sub>2</sub> hydrates formation  
117 and dissociation in porous media using a calorimetric approach. Several studies attempted to  
118 investigate the interaction between gas hydrates and the porous media in which they form  
119 (Adeyemo et al., 2010; Bagherzadeh et al., 2011; Chong et al., 2016; Fitzgerald et al., 2014; Ge  
120 et al., 2019; Heeschen et al., 2016; Kang et al., 2013; Kumar et al., 2015; Mekala et al., 2014;  
121 Nguyen et al., 2020; [Qin et al., 2022](#); Smith et al., 2002; [Wang et al., 2021](#); [Zhang et al., 2022](#);  
122 Zhang et al., 2016). This literature draws attention to the effect of several factors on gas hydrate  
123 formation rate and water to hydrate conversion, such as:

124 (1) The nature of porous media (surface chemistry, morphology: pore and particle size). Indeed,  
125 for particle size, a number of studies demonstrated an increase in the amount of hydrates  
126 formed, with higher gas consumption by hydrates and/or higher water-to-hydrate conversion  
127 rate for smaller particle sizes tested (Bhattacharjee et al., 2015; Ge et al., 2019; Mekala et al.,  
128 2014). For example, Ge et al. (2019) performed CH<sub>4</sub> hydrate formation in a high-pressure  
129 reactor using two particle size classes of silica sand, 180-250 and 300-900 μm. The porous  
130 media was 70 % saturated with pure water. The authors demonstrated higher gas consumption  
131 by hydrates and water-to-hydrate conversion for the smallest particle size. This tendency is also  
132 observed for smaller pore sizes (Zhang et al., 2015). However, other studies demonstrated an  
133 opposite result concerning the influence of particle size (Kumar et al., 2015; Lu et al., 2011;  
134 Pan et al., 2018). In fact, Pan et al. (2018) performed CH<sub>4</sub> hydrate formation in silica sand for  
135 various particle sizes, 38, 48, 74, 106 and 165 μm. In their study, they used a 300-ppm (mass  
136 fraction) [of sodium dodecyl sulfate \(SDS\)](#) solution for all experiments with a liquid phase

137 saturation of 50 %. The results showed that gas storage capacity and water to hydrate  
138 conversion rate increase with the increase of particle size (0.101 mol of gas/mol of liquid and  
139 61.9 % water to hydrate conversion rate for 38  $\mu\text{m}$  particle size, versus 0.151 mol of gas/mol  
140 of liquid and 92.2 % water to hydrate conversion rate for 165  $\mu\text{m}$  particle size). The authors  
141 suggested that smaller particle sizes lead to narrow pores, which can decrease connectivity of  
142 the porous media, and slower  $\text{CH}_4$  diffusion in the liquid phase. Globally, it has been suggested  
143 that hydrates formed in smaller pores may obstruct gas diffusion in the porous media.

144 (2) The operating conditions (pressure, temperature, water saturation, gas solubility, etc.).  
145 Indeed, several studies have shown that water saturation affects not only the final hydrate  
146 saturation, but also the gas transport within the porous medium (Babu et al., 2013; Bagherzadeh  
147 et al., 2011; Ge et al., 2019; Kumar et al., 2015). Some of these studies have shown that at low  
148 water saturation, gas transport in the pore medium is facilitated, and liquid-gas contact is  
149 improved. As a consequence, the formation of hydrates is also improved. However, some  
150 authors have shown that low water saturation limits the amount of water available for hydrate  
151 formation (Babu et al., 2013; Kumar et al., 2015). Based on the above studies, it is noted that  
152 water saturation is an important factor that requires further and extensive studies to determine  
153 the optimal water saturation conditions for gas hydrate formation in the studied porous media.

154 Obviously, the effects of porous structure on gas hydrates formation kinetics, particularly on  
155 induction time, are not fully understood, as well as, the effect of the nature of porous media on  
156 gas-liquid contact area and on heat/mass transfer.

157 To better control gas hydrates formation and dissociation in a cold storage system, it is of great  
158 interest to study  $\text{CO}_2$  hydrate formation kinetics and their thermodynamic stability conditions,  
159 as well as the possible energy storage of the porous media containing  $\text{CO}_2$  hydrates. The present  
160 paper aims to provide further insight into  $\text{CO}_2$  hydrate formation and dissociation processes in  
161 porous media based on heat and mass transfer characterization. Using a differential thermal

162 analysis method, an original approach in literature to study CO<sub>2</sub> hydrates in porous media for  
163 cold storage purpose, the effect of key factors such as water saturation, particle size and the  
164 morphology of the porous media on the solid mass fraction formed was investigated. For the  
165 latter, two morphologically different porous media were used: silica sand and **dual porous** silica  
166 gel. The experimental data obtained add to a growing body of literature on the influence of  
167 porous media on gas hydrate formation and dissociation processes, in an attempt to enhance  
168 energy efficiency of industrial applications such as hydrate-based cold storage systems.



## 169 2. Experimental section

170 CO<sub>2</sub> hydrates formation and dissociation experiments were conducted using differential thermal  
 171 analysis, which is an accurate and suitable method of characterizing thermal properties such as  
 172 dissociation enthalpy of gas hydrates. This heat-flux calorimetry method is traditionally used  
 173 to measure various thermo-physical properties of gas hydrates (Gupta et al., 2008; Kang et al.,  
 174 2001; Lievois et al., 1990). The principle is based on the use of two identical cells connected to  
 175 each other by several thermocouples. This connection allows an instantaneous and precise  
 176 measurement of the temperature change between the two cells when a phase change occurs in  
 177 one of the cells. A detailed description of the method is given in the following subsections.

### 178 2.1. Materials

179 Carbon dioxide with a certified purity of more than 99.7 % was supplied by Linde Gas (France).  
 180 Fontainebleau silica sand purchased from Laboratoires Humeau (La Chapelle-sur-Erdre,  
 181 France) and spherical silica porous gel particles of nominal pore diameters of 30 and 100 nm  
 182 supplied by Silicycle Co. (Canada) were used as porous media. All materials were used without  
 183 further purification. The detailed properties of silica sand and silica gel are listed in Table 1.

184 Table 1: Physical properties of Fontainebleau silica sand and silica gel samples.

Parameters	Fontainebleau silica sand	30 nm Silica gel	100 nm Silica gel
Mean particle diameter ( $\mu\text{m}$ )	80-450	20-45	20-45
Mean pore diameter (nm)	-	30	100
Pore volume ( $\text{cm}^3 \cdot \text{g}^{-1}$ )	-	0.86	0.7
Dry density ( $\text{g} \cdot \text{cm}^{-3}$ )	2.65	2.2	2.2

185 To study the influence of particle size on CO<sub>2</sub> hydrate formation and dissociation,  
 186 Fontainebleau silica sand was sieved to 3 classes of particles: 80 to 160  $\mu\text{m}$ ; 160 to 315  $\mu\text{m}$  and  
 187 315 to 450  $\mu\text{m}$  noted respectively PS01, PS02 and PS03.

## 2.2. Differential thermal analysis (DTA) apparatus description

188 A differential thermal analysis (DTA) apparatus was used for the experiments, whose principle  
189 was described in a previous work (Fournaison et al., 2004). It was designed to measure the  
190 difference in thermal behavior between two identical cells submitted to the same heat flux. A  
191 schematic diagram of the experimental apparatus is shown in Figure 1. It consists of two  
192 identical and symmetric transparent glass cells with a functional volume of 40 ml. The  
193 transparent walls enable visualization of the studied samples inside the cells.  
194 The two cells are immersed in a temperature-controlled bath (blue area in Figure 1). One of  
195 them is filled with the porous media **at a certain water saturation** and used as the reactor for  
196 hydrate formation (called measurement cell). The second cell (called reference cell) is filled  
197 with the same porous media and **water saturation as the measurement cell** with an inert solution  
198 of water-ethanol 50 % vol/vol, **in order to avoid crystallization during the thermal cycle while**  
199 **having thermal properties close to those of the liquid in the measurement cell**. The measurement  
200 cell is connected to a CO<sub>2</sub> supply line, which contains a cylinder with a volume of 10 cm<sup>3</sup>  
201 ( $\pm 10$  % tolerance on the volume) and three manual valves to allow gas supply. The cylinder is  
202 also immersed in the temperature-controlled bath. It allows (1) to determine the amount of gas  
203 injected in the measurement cell and (2) to limit the risk of overpressure in the glass cell. Indeed,  
204 CO<sub>2</sub> is injected in the measurement cell using a successive gas expansion method. This method  
205 consists of injecting the gas into the sample cylinder while keeping valve 1 closed. Valve 3 is  
206 then closed to disconnect the gas supply. Once the pressure in this circuit is stable, valve 1 is  
207 open to allow gas expansion in the cell. This operation is repeated several times until the  
208 targeted experimental pressure around 2.5 MPa is reached. The amount of CO<sub>2</sub> injected (mole)  
209 in each operation is calculated by the difference between the amount of CO<sub>2</sub> (mole) present in  
210 the circuit (between valve 1 and valve 3) before and after expansion to the cell.  
211

212 The pressure is measured at two points: the first pressure sensor (0-10 MPa. 0.011 % full scale.  
213 Keller) is located at the inlet of the measuring cell, and a second one (0-10 MPa. 0.006 % full  
214 scale. Keller) at the inlet of the gas supply line.

215 Each cell is equipped with one thermocouple that gives a direct temperature measurement  
216 ( $\pm 0.5$  K). The DTA measurement is based on the use of six thermocouples, three of which are  
217 inserted in one cell and three in the other. All thermocouples are located at the lowest part of  
218 the cell. These six thermocouples are connected together in series, by a back and forth  
219 connection between the two cells, as shown in Figure 2. This connection makes it possible to  
220 obtain an electrical signal directly linked to the difference in temperature between the two cells,  
221 and consequently to the difference in heat flow, knowing that the two cells are immersed in the  
222 same temperature-controlled bath.

223 The first advantage of this direct connection between the two cells is to allow an "instantaneous"  
224 measurement of the temperature difference, and not a difference between two temperature  
225 values measured by two individual thermocouples (which would each imply a measurement  
226 error). Another interest of the back and forth connection is to amplify the differential signal  
227 between the two cells, while limiting the error to one measurement, i.e. the signal recovered by  
228 the acquisition unit. This avoids the cumulative errors that could be obtained if six  
229 thermocouples were used individually.

## 230 **2.3.Experimental procedure**

### 231 **2.3.1. Sample preparation and characterization**

232 Silica sand samples at various water saturation were prepared using the following procedure:  
233 first, silica sand was dried at 388.15 K for 24 h. Then an amount of water corresponding to the  
234 desired water saturation was added to the sand at ambient temperature. The porosity of the  
235 unpacked sand was estimated by the supplier (Humeau Laboratories) to be approximately 0.44.  
236 Finally, the mixture was introduced into the measurement cell and packed evenly to fill the

237 entire volume. In order to evaluate the water distribution in the sand samples, an X-ray micro-  
 238 tomography experiment (DeskTom 130®, RX Solution, Chavanod, France) was performed on  
 239 a sand sample with 66 % water saturation. The sample was prepared under the same conditions  
 240 as the hydrate formation experiments, but in a transparent resin cell (Formlabs, Clear  
 241 PhotoPolymer) which has the same internal volume as the DTA cells (inner diameter = 3 cm,  
 242 height = 6.4 cm). This sample was then placed in the micro-tomography device.

243 The analysis was performed with a voltage of 124  $\mu\text{V}$  and a voxel size of 27.33  $\mu\text{m}$ . XAct 2®  
 244 software (RX Solution, Chavanod, France) was then used for 3D-reconstruction from raw  
 245 images. A 3D-visualization and volume fractions of the phases within the sample (sand, water  
 246 and air) were obtained using Avizo 2019.1® software (Thermo Fisher Scientific, Waltham,  
 247 USA). Figure 3 shows the images obtained after the 3D-reconstruction. Due to the size of the  
 248 sample, which produces a very large data file, the image processing was performed on two  
 249 volumes (clipped) located in the upper and lower part of the sample. The idea was to have a  
 250 clearer view on the water distribution over the sample. The latter contains three phases; sand  
 251 (represented in yellow), water (blue) and air (dark grey). **Table 2** shows information about the  
 252 volume fractions of the different **compounds** contained in the selected parts.

253 Table 2: Volume fractions of air, water and **packed** silica sand within the analyzed volumes  
 254 **by micro-tomography**

<b>Analyzed Volume</b>	<b>Material</b>	<b>Volume fraction (%)</b>	<b>Total volume (cm<sup>3</sup>)</b>
<b>Upper part</b>	Air	0.10	0.529
	Water	0.19	
	Silica Sand	0.71	
<b>Lower part</b>	Air	0.10	0.190
	Water	0.19	
	Silica Sand	0.71	

255 Overall, based on Figure 3 and **Table 2** analysis, it can thus be reasonably assumed that the  
 256 filling method used for silica sand samples leads to a homogeneous **water dispersion in the**

257 porous media since the same distribution of the various compounds was observed by micro-  
258 tomography at different spatial positions of the sample.

259 In order to address the limitations related to the mass transfer of gas, and water-gas contact in  
260 the porous media, and in light with previous studies (Adeyemo et al., 2010; Dicharry et al.,  
261 2013; Kang et al., 2008; Kumar et al., 2013; Park et al., 2006), it seems to be important to study  
262 media with different morphologies (presence or not of dual porosity), in order to enhance the  
263 amount of energy stored per volume. In fact, dual porosity media may present two advantages  
264 for cold storage system:

265 1) Provide an additional internal surface area,

266 2) Provide a better diffusion of gas through the porous media, since water can occupy the  
267 internal pore volume thanks to capillary forces, thus leaving the interstitial space potentially  
268 free for gas diffusion (as represented by the schematic illustration in Figure 4).

269 Silica gel samples were prepared using a procedure from Dicharry et al. (2013). The procedure  
270 consists of layering uniformly the dried silica gel and water at 393.15 K for 24 h in various  
271 stages alternatively. The amount of water introduced at each layer is identical to the desired  
272 saturation of the pore volume of silica gel. The same procedures (for sand or silica gel) were  
273 used to fill the reference cell. Finally, the measurement cell was closed and residual air was  
274 removed with a vacuum pump.

### 275 **2.3.2. DTA analysis of CO<sub>2</sub> hydrate formation and dissociation in** 276 **silica sand**

277 After pressurizing the measurement cell with CO<sub>2</sub> using an expansion method to the desired  
278 experimental pressure set around 2.5 MPa, the bath temperature was then set to 285.15 K to  
279 stabilize the temperature inside both cells at an initial equilibrium state. Figure 5 shows the  
280 evolution of pressure, temperature and DTA signal during an experiment in sand initially

281 saturated with water at 33 %. After the initial equilibrium state, the system was gradually cooled  
282 down until 271.15 K.

283 The temperature peak (red line) indicates CO<sub>2</sub> hydrate formation due to the exothermic property  
284 of crystallization. Meanwhile, the DTA signal peak (blue line) illustrates the difference in heat  
285 transfer between the two cells. Thus, when the temperature conditions are close in both cells,  
286 the DTA signal is close to zero. However, when the exothermic reaction occurs in the  
287 measurement cell, the DTA signal increases rapidly with a similar pattern compared to the  
288 direct measurement of the temperature. CO<sub>2</sub> hydrate formation is also accompanied with a  
289 temperature peak and a strong decrease in the system pressure due to the consumption of CO<sub>2</sub>  
290 during the hydrate growth. **Figure 5b shows the presence of two consecutive DTA peaks (2 red**  
291 **arrows on Figure 5b). These two peaks are accompanied with 2 consecutive pressure drops**  
292 **corresponding to gas consumption by hydrates. This result suggests the occurrence of multiple**  
293 **nucleation followed by growth of CO<sub>2</sub> hydrates in silica sand. This behavior occurred for all**  
294 **experiments within silica sand.** When pressure, temperature and DTA signal stabilized the  
295 thermodynamic equilibrium was considered to be reached, and CO<sub>2</sub> hydrate formation finished.  
296 Hydrate dissociation was triggered by increasing the bath temperature gradually with a rate of  
297 0.1 K.min<sup>-1</sup> until the initial temperature was reached (285.15 K). As shown in Figure 5a and c,  
298 hydrate dissociation is expressed by a large and opposite variation in the DTA signal compared  
299 to hydrate formation. This is due to the endothermic nature of hydrate dissociation. The  
300 temperature condition was then maintained at 285.15 K to ensure a complete hydrate  
301 dissociation. Due to **supercooling** phenomena related to the crystallization of gas hydrates, the  
302 exploitation of the DTA signal peak related to hydrate formation remains difficult. **Indeed, the**  
303 **formation being done by breakage of supercooling, in bulk and porous media, but with higher**  
304 **driving force, in porous media, the formation peaks quality strongly depends on the operating**  
305 **conditions.** For this reason, dissociation peaks are generally used in calorimetry work (Chami

306 et al., 2021; Lin et al., 2014). Thus, the discretization of the DTA signal obtained during hydrate  
307 dissociation was performed to determine the experimental dissociation enthalpy and calculate  
308 the mass of hydrates formed in the reactor.

### 309 **2.3.3. Effect of the pore size of silica gel on equilibrium conditions of** 310 **CO<sub>2</sub> hydrates**

311 The effect of dual porous silica gel on the thermodynamic conditions of hydrate stability was  
312 examined. Figure 6a presents the results related to dissociation temperature of CO<sub>2</sub> hydrates in  
313 silica gel with a pore volume of 100 nm and 30 nm. These results are plotted in a *P-T* diagram  
314 and compared to the bulk-CO<sub>2</sub> equilibrium curve. A shift can be seen between the bulk-CO<sub>2</sub>  
315 hydrate equilibrium curve and that obtained in silica gel with a nominal pore size of 100 nm  
316 and 30 nm. For instance, with a pressure of 1.46 MPa, the two equilibrium temperatures present  
317 a shift of 0.7 K towards lower temperature conditions in comparison with the bulk equilibrium  
318 curve. Figure 6b shows that these results are consistent with those reported in the literature  
319 using several pore sizes of silica gel. All three-phase equilibrium points of CO<sub>2</sub> hydrates in  
320 silica gel with varying nominal pore sizes show a deviation from the bulk equilibrium curve of  
321 CO<sub>2</sub> hydrates. In addition, a decrease in pore size (going from 100 to 30 and then to 15 nm)  
322 resulted in a higher shift from the CO<sub>2</sub> hydrate equilibrium curve. In general, the presence of  
323 mesoporous volume from the ten to fifty nanometer scale generates an inhibiting effect for the  
324 formation of hydrates in silica gel. This can be explained by an important capillary effect  
325 generated by small pore size. Indeed, water being confined in very small pore size leads to a  
326 high capillary pressure. Consequently, the system needs more energy in order to overcome these  
327 forces and form hydrates in the mesoporous volume. This result is also demonstrated in several  
328 previous studies for CO<sub>2</sub>, CH<sub>4</sub> and C<sub>3</sub>H<sub>8</sub> (Adeyemo et al., 2010; Babu et al., 2013; Dicharry et  
329 al., 2013; Handa and Stupin, 1992; Smith et al., 2002; Turner et al., 2005; Uchida et al., 2002;  
330 Yang et al., 2012).

### 2.3.4. Calibration and quantification of the amount of CO<sub>2</sub> hydrates formed

331 It is important to mention that the DTA technique is based on the determination of relative  
 332 properties that depend on the heat transfer between the bath and the measurement/reference  
 333 cell, which is related to the system configuration and geometry. Therefore, a calibration  
 334 experiment consisting of formation and dissociation procedure applied to a calibration material  
 335 with known properties is required for each new configuration (the geometric characteristics,  
 336 nature of the porous media, water saturation, etc.). In **this** case, the calibration material is ice  
 337 since its thermal properties are well known. This calibration experiment is based on the same  
 338 procedure as for hydrate formation but without the gas injection step. The integration of the  
 339 DTA peak during ice melting is used to determine a calibration coefficient  $C_{ice}$ . This coefficient  
 340 is used to calculate the amount of energy consumed by hydrate dissociation as follows:

$$E_{exp}(kJ) = |C_{ice} * A_{hyd}| \quad (1)$$

343  $A_{hyd}$  represents the result of the integration of the DTA signal peak related to hydrate  
 344 dissociation. The mass of hydrates formed is computed using the experimental enthalpy  
 345 obtained by equation (1) and the theoretical enthalpy of gas hydrates  $\Delta H_{hyd}$  known to be equal  
 346 to 500 kJ/kg<sub>water</sub> (374 kJ/kg<sub>hydrates</sub>) (Anderson, 2003; Fournaison et al., 2004):

$$m_{hyd}(kg) = \frac{E_{exp}}{\Delta H_{hyd}} \quad (2)$$

347 This equation does not take into account the variation over time of the difference in sensible  
 348 heat between the two cells. This variation only implies an error of approximately 2% on the  
 349 total amount of heat exchanged.

350 Water to hydrate conversion rate is computed from the following equation:

$$C_{wh} (\%) = \frac{m_{hyd} * n_h * M_{H_2O}}{\rho_{hyd} * m_{H_2O}} * 100 \quad (3)$$



351 Hydration number  $n_h$  used for the present study is 7.23 (Kang et al., 2001),  $\rho_{hyd}$  is the density  
352 of CO<sub>2</sub> hydrate computed using the previous hydration number and  $m_{H_2O}$  is the mass of water  
353 introduced initially in the porous media.

### 354 **3. Results and discussion**

355 The efficiency of cold storage system using gas hydrates is related not only to thermodynamic  
356 equilibrium conditions, but also to gas hydrates formation and dissociation kinetics, and  
357 ultimately to the amount of cold thermal energy that can be stored and released per volume unit.  
358 In this study, the DTA apparatus described in the previous section was used to investigate  
359 particularly the effect of key factors related to the geometric characteristics of porous media  
360 and the operating conditions (water saturation, particle size and the morphology of the porous  
361 media) on the following storage properties:

- 362 1) The mass of CO<sub>2</sub> hydrates formed in the porous media determined by measuring the  
363 heat consumed during gas hydrate dissociation. It is of importance to identify the factors  
364 that influence the amount of hydrate formed, and thus, the amount of energy available  
365 in a cold storage system.
- 366 2) The induction time where no significant macroscopic changes are observed. It  
367 corresponds to the period between the moment when the system reaches the CO<sub>2</sub>  
368 hydrates bulk Hydrate-Liquid-Vapor equilibrium conditions (Sloan and Koh, 2007)  
369 (which are considered as reference equilibrium conditions) and the moment when a  
370 rapid hydrate crystal growth is detected. The induction time is a significant index when  
371 studying hydrate growth kinetics. It is well known in the literature that induction time  
372 measurements can be relatively difficult due to the stochastic nature of hydrate  
373 nucleation (Bishnoi and Natarajan, 1996; Dai et al., 2014; Lee et al., 2013). In addition,  
374 several studies showed the link between induction time and the driving force applied to  
375 the system (temperature driving force or supercooling, pressure driving force and mass-

376 transfer driving force) (Davies et al., 2009; Kashchiev and Firoozabadi, 2002; Liu et al.,  
 377 2015; Natarajan et al., 1994; Skovborg et al., 1993). However, the effect of other factors  
 378 related to the characteristics of the porous media, like water saturation, particle size, or  
 379 the presence of a mesoporous space are still poorly understood.

### 380 3.1. Impact on amount of hydrates formed

#### 381 3.1.1. Effect of water saturation

382 The influence of water saturation on the mass of gas hydrates formed was first investigated  
 383 based on a set of experiments on silica sand with various water saturation conditions and  
 384 particle size. Table 3 summarizes the experimental conditions applied to this set of experiments  
 385 and the final water to hydrate conversion (based on the fixed hydration number of CO<sub>2</sub> hydrate).  
 386 Water content is defined as the mass of water by the mass of solid particles (sand grains or  
 387 Silica gel particles) initially introduced in the cell.

388 Table 3: CO<sub>2</sub> hydrate formation and dissociation results in a sandy matrix for several water  
 389 saturations and particle size

Run	Sample state*	Particle size (µm)	Water mass (g)	Water saturation (%)	Mass of Solid particles (g)	Water content	Mass of hydrates formed (g)	Water conversion to hydrate (%)
1	F	Non-sieved sand	5.78	33.4	59.58	0.10	3.17	41.2
2	F		9.00	52.0	59.57	0.15	3.39	28.1
3	F		11.05	59.9	56.60	0.19	3.20	21.8
4	F		11.32	63.7	58.37	0.19	1.87	12.5
5	M		11.32	63.7	58.37	0.19	2.27	14.9
6	F		13.10	75.2	59.31	0.22	2.16	12.3
7	F		17.45	100	59.36	0.29	No hydrate formation succeeded	
8	F	PS01	10.34	53.4	54.16	0.19	4.47	32.3
9	F	PS02	9.37	51.5	57.15	0.16	3.60	28.7
10	F	PS03	9.20	51.8	58.36	0.16	3.16	25.7

390 \*F: fresh sample. M: memory sample. In the latter state, Run 5 represents a repeatability test for Run 4  
 391 (without changing the sample).

392 The influence of water saturation on the amount of hydrates formed is also represented in  
 393 Figure 7, with the mass of the hydrate formed and the rate of water to hydrate conversion as a  
 394 function of water saturation of non-sieved silica sand. It is interesting to note that the amount

395 of hydrates formed is not significantly different for water saturations ranging from 33 to 60 %.  
396 However, for higher water saturation (63 % and higher), the results show lower values of the  
397 mass of hydrates formed. It is also interesting to note that the rates of water conversion to  
398 hydrates are between 12 and 41 % and follow a decreasing tendency with the increase of water  
399 saturation. This is due to the fact that in the measurement cell the formation of hydrates takes  
400 place in a closed system after CO<sub>2</sub> injection. In fact, the gas first dissolves in water under  
401 temperature conditions outside the hydrate stability zone. After reaching a stable saturation,  
402 which corresponds to the same ( $P$ ,  $T$ ) conditions for all experiments, the system is closed. Thus,  
403 knowing that the density of CO<sub>2</sub> in vapor phase is higher than the density of CO<sub>2</sub> dissolved in  
404 liquid phase, the total amount of CO<sub>2</sub> in the system also decreases when increasing water  
405 saturation (and so decreasing the volume of the vapor phase). After closing the system, the  
406 temperature is decreased to form hydrates. With less CO<sub>2</sub> available in the system, and more  
407 water, then less hydrate is formed, as confirmed by the results from a previous solid fraction  
408 model based on an equilibrium balance on CO<sub>2</sub> in its different vapor, dissolved in liquid and  
409 hydrate phases (Marinhas et al., 2007). It is interesting to note that these mass balance results  
410 are in the same range of values as the present results from the calorimetric approach as seen in  
411 Figure 7 with the open and full green diamonds.

412 Another aspect that must be taken into consideration when investigating the effect of water  
413 saturation on gas hydrate formation is the spatial distribution of water in the porous volume.  
414 Under high water saturation conditions, the distribution of liquid and vapor phases limits the  
415 interfacial contact, and sometimes leads to the formation of hydrate plugs. This can prevent the  
416 gas from accessing certain water zones in the pores. On the other hand, at low water saturation,  
417 gas diffusion through the porous medium is facilitated due to a relatively larger void volume.  
418 For experiment 7 where silica sand is completely saturated with water ( $S_w = 100\%$ ), the DTA  
419 peak of hydrate formation was not detected and no pressure drop was observed despite a

420 relatively long experiment time (52 h). Indeed, the desired experimental pressure (2.5 MPa)  
421 could not be reached within a reasonable time. This result suggests that with a saturated porous  
422 media, liquid-gas contact area through which CO<sub>2</sub> diffuses in water is reduced. In addition,  
423 given that water occupies the total pore volume, the amount of CO<sub>2</sub> initially injected to reach  
424 the same experimental pressure conditions is reduced. Consequently, hydrate formation is  
425 hindered.

426 Overall, **these** findings confirm the existence of a strong correlation between water saturation  
427 and the amount of CO<sub>2</sub> hydrate formed, as it is reported in previous studies for CH<sub>4</sub> hydrates in  
428 several porous media (Babu et al., 2013; Bagherzadeh et al., 2011; Ge et al., 2019; Kumar et  
429 al., 2015; Pan et al., 2018). As the focus of this study is to appreciate optimal water saturation  
430 conditions for an efficient cold storage system, the results demonstrate that a 50-60 % water  
431 saturated system could be a suitable level to maximize the amount of energy stored. **This**  
432 **optimal saturation value is slightly lower than the value usually used in the literature to improve**  
433 **hydrate formation kinetics around 70 % (Ge et al., 2019; Mekala et al., 2014).** However, further  
434 investigations should be carried out to study additional water saturations. Moreover, a semi-  
435 batch configuration where CO<sub>2</sub> is continuously injected during hydrate formation should be  
436 tested. Indeed, this gas-excess configuration could increase the amount of hydrate formed and  
437 potentially the water to hydrate conversion rate. **These** results also suggested that hydrate  
438 conversion rate could be influenced by the spatial distribution of water in the pore volume. The  
439 latter is strongly related to the geometric characteristic of the porous media, which will be  
440 discussed in the following section.

### 441 **3.1.2. Effect of particle size**

442 **For the study of the effect of particle size on CO<sub>2</sub> hydrate formation and dissociation in porous**  
443 **media, Fontainebleau Silica sand was sieved into 3 particle size classes: PS01, PS02 and PS03.**  
444 **Figure 8 shows the evolution of the formed hydrate mass and water to hydrate conversion rates**

445 as a function of the particle size classes for a given water saturation around 52.2 %  
446 corresponding to runs 8 to 10 in Table 3. The pore volume for the particle size classes being the  
447 same, the same quantity of water is used in the various sand samples. A clear decreasing  
448 tendency of the amount of hydrate mass and hydrate conversion rate as a function of the four  
449 particle size classes is observed. This pattern is due to the decrease of the specific area resulting  
450 from the increase of particle size. Indeed, for a larger specific area (smaller particle size) water  
451 is adsorbed on a larger surface area. This could potentially enhance the liquid-gas contact area,  
452 which can improve gas hydrate formation. This suggests that CO<sub>2</sub> hydrate formation occurs  
453 preferentially at the solid-liquid interfaces of sand particles. It is important to note that the mass  
454 of hydrates obtained within the non-sieved sand is close to the amount within PS02 because  
455 this class represents 80 % of the non-sieved sand. Alternatively, it is possible to assume that the  
456 fraction leftover representing 10 % has no significant influence on the hydrate conversion rate.

457 These findings are consistent with some previous studies reported in the literature  
458 (Bhattacharjee et al., 2015; Ge et al., 2019; Mekala et al., 2014; Qin et al., 2022) and mentioned  
459 in the introduction section. However, other studies demonstrated an opposite result (Adeyemo  
460 et al., 2010; Kumar et al., 2015; Lu et al., 2011; Pan et al., 2018). In this case, it has been  
461 suggested, globally, that hydrates formed in smaller pores may obstruct gas diffusion in the  
462 porous media. In their recent review Qin et al. (2021) also reported this inconsistency between  
463 previous studies on the influence of particle size on hydrate formation. Indeed, the authors  
464 suggested that this discrepancy in the results of the above-mentioned studies might be due to  
465 the influence of other factors, such as the initial water saturation used in each study, the  
466 composition of the gas phase, the specific surface area, or even the experimental system and  
467 hydrate formation procedure used. Overall, further studies are needed, especially for CO<sub>2</sub>  
468 hydrates, considering the above-mentioned cross-factor effect to better understand the

469 mechanisms involved in order to determine the influence of particle size on gas hydrates  
470 formation.

### 471 **3.1.3. Effect of the morphology**

472 In this section, results from the investigation of CO<sub>2</sub> hydrate formation and dissociation in two  
473 morphologically different porous media, silica sand and silica gel, are reported. Fontainebleau  
474 silica sand is considered as a uniform grain size structure (with only external porosity) and silica  
475 gel as a dual porosity media (with internal and external porosity). The data of mass hydrate  
476 formed and water to hydrate conversion rates are illustrated in Table 4. They are presented for  
477 dual porous silica gel with two distinct pore size and compared with the results obtained in  
478 Fontainebleau silica sand (detailed properties in the experimental section, Table 1).

479 For silica gel samples, three configurations of water saturation were tested:

- 480 1) Amount of water injected lower than the internal pore volume  $V_w < V_p$  (Run 1 and 2)
- 481 2) Amount of water injected corresponding to the internal pore volume  $V_w = V_p$  (Run 3, 4  
482 and 6)
- 483 3) Amount of water injected greater than the pore volume  $V_w > V_p$  (Run 5, 7 and 8); in this  
484 case, it is assumed that the water occupies the entire internal pore volume, but also a  
485 fraction of the interstitial space (external pore).

486 The water saturation of the internal pore volume of silica gel and of the interstitial space are  
487 respectively denoted  $Sw_p$  and  $Sw_i$ .

488

489

Table 4: CO<sub>2</sub> hydrate formation and dissociation results in silica gel

Run	Pore size (nm)	Mass of water injected (g)	Water saturation of Pore volume $Sw_p$ (%)	Water saturation of Interstitial space $Sw_i$ (%)	Mass of solid particles (g)	Water content	Induction time (min)	Mass of hydrate formed (g)	Water to hydrate conversion rate (%)
1	100	5.93	53	0	15.99	0.37	No hydrate		
2		9.01	78	0	16.46	0.55	165	4.63	38.4
3		11.35	100	0	16.22	0.70	203	4.70	30.9
4		11.01	100	0	15.73	0.70	102	4.83	32.8
5		17.98	100	32	16.00	1.12	82	2.68	11.1
6	30	14.10	100	0	16.42	0.86	100	4.52	24.0
7		19.47	100	30	16.17	1.20	740	5.02	19.3
8		21.83	100	43	16.00	1.36	253	2.45	8.4

490 First, a comparison of hydrate formation and dissociation DTA signals obtained in both silica  
491 sand and silica gel with close initial water mass is illustrated in Figure 9 (for clarity, DTA peaks  
492 are overlapped). It should be noted that the DTA signal is a differential measurement between  
493 the two cells, and as mentioned earlier in this paper, the reference cell contains the same porous  
494 media as in the measurement cell for each experiment. Therefore, it can reasonably perform a  
495 comparative analysis of the DTA peaks without considering the difference in thermal  
496 conductivities of the two porous media (silica sand and silica gel). From Figure 9, it is  
497 interesting to notice higher and larger exothermic and endothermic DTA signal peaks for the  
498 experiments performed in silica gel compared to silica sand. This measurement indicates a  
499 significant difference in thermal behavior between the test cell and the reference cell in the case  
500 of silica gel compared to silica sand, thus, a greater amount of thermal energy stored/released  
501 in the silica gel media compared to silica sand. These results suggest a strong effect of the  
502 structural organization (morphology and water distribution) of the porous media on heat transfer  
503 in the system. Moreover, DTA signals for the majority of experiments performed in silica gel  
504 did not show a smaller second formation peak, except for one experiment in 100 nm pore size

505 silica gel (Run 3, 4). Whereas, all the experiments carried out in silica sand showed a multiple  
506 nucleation phenomenon expressed by the presence of a second DTA signal peak of very small  
507 intensity. It could be conceivably hypothesized that this difference may be related to the shape  
508 of the particles. Indeed, silica gel particles have a spherical shape compared to sand particles,  
509 which have rather irregular shapes. In the latter, the morphology of the void space could be  
510 more heterogeneous compared to a silica gel porous media. Thus, mass transfer could be  
511 affected by this heterogeneity, which can lead to multiple nucleation loci at delayed times. The  
512 amount of hydrate formed under several water saturation conditions of silica gel, and in the two  
513 distinct pore sizes, was then examined. The results of hydrate mass formed and water to hydrate  
514 conversion rates are shown in Table 4 and Figure 10. Globally, it can be seen from Figure 10  
515 that the hydrate mass in silica gel, as well as water to hydrate conversion rates, are higher in  
516 comparison with silica sand. However, this difference is not in the same order of magnitude as  
517 DTA signal peaks shown in Figure 9. This is due to ice calibration (used to calculate the mass  
518 of hydrates formed) which is different, depending on the system configuration. In addition, the  
519 results indicate that a configuration of the system where water occupies only the pore volume  
520 of silica gel, water content lower than 1, seems to be a good option to enhance the amount of  
521 hydrate formed. This can be explained by the presence of a mesoporous volume in silica gel,  
522 which seems to enhance gas and water contact. Indeed, water can be adsorbed at the surface of  
523 silica gel inside the pores thanks to capillary forces, which leaves the interstitial space free for  
524 a better diffusion of gas through the porous media. Regarding water to hydrate conversion rate,  
525 the results show a decreasing tendency when the initial amount of water increase in the system.  
526 As it is observed in silica sand, when the amount of water in silica gel increases, it results in a  
527 decrease in the amount of CO<sub>2</sub> initially injected in the measurement cell of the DTA apparatus.  
528 Furthermore, when the water content is higher than 1 in silica gel, that means the water amount  
529 is sufficient to saturate not only the pore volume but also the interstitial space, the system



530 configuration is closed to that obtained in silica sand and the amount of hydrate formed are  
 531 comparable in some cases. In this case, the formation of the hydrate could be affected by the  
 532 heterogeneous distribution of water and gas in the porous media. This can explain the decrease  
 533 in the amount of hydrate formed observed with both pore size of silica gel (100 nm and 30 nm).

### 534 3.2. Impact on induction time

#### 535 3.2.1. Effect of water saturation

536 The influence of water saturation on induction time was first investigated based on a set of  
 537 experiments on silica sand with various water saturation conditions and particle size. Table 5  
 538 summarizes the experimental conditions applied to this set of experiments.

539 Table 5: Induction time of CO<sub>2</sub> hydrate formation and dissociation results in a sandy matrix

Run	Particle size	Water saturation (%)	Induction time (min)	Driving force (% mol CO <sub>2</sub> /mol H <sub>2</sub> O)
1	Non-sieved sand	33.4	68	0.59
2		52.0	51	0.67
3		59.9	120	0.84
4		63.7	83	0.73
5		63.7	399	0.72
6		75.2	81	0.71
7		100	No hydrate formation succeeded -	
8	PS01	53.4	87	0.86
9	PS02	51.5	83	0.83
10	PS03	51.8	92	0.85

540 Figure 11a shows the induction time values obtained as a function of water saturation of the  
 541 porous sample in the cell. To our knowledge, induction time data for CO<sub>2</sub> hydrates as a function  
 542 of water saturation of the porous media are poorly known. **Some authors provided induction**  
 543 **time data for CO<sub>2</sub> hydrate formation in different porous media but at a unique water saturation**  
 544 **(Rehman et al., 2022; Sahu et al., 2022) and these data are added to figure 11a for comparison.**  
 545 The induction time values are scattered and vary between 51 and 120 min for the majority of  
 546 the experiments **except for Sahu et al. (2022). They showed an important induction time of**  
 547 **2083.8 min within a silica sand of 0.15 mm particle diameter at 70 % water saturation.** The

548 induction time dispersion may be due to several key factors such as the configuration of the  
549 experimental system (reactor type and design, the internal volume, operating conditions,  
550 driving force...). There are therefore biases of interpretation when different works are  
551 compared. A slight increase of induction time can be observed when water saturation of silica  
552 sand increases. However, for the repeated experiment at 63.7 % water saturation (Run 5, 5) (for  
553 this experiment, the sample was left about 210 min at 285 K before restarting the cooling  
554 process), it can be noted a considerable difference in the induction time compared to the rest of  
555 the experiments. This discrepancy in induction time may be related to a heterogeneous  
556 redistribution of the water within the porous media after hydrate dissociation. Indeed, the CO<sub>2</sub>  
557 hydrate formation experiments in this study are performed for an experimental temperature of  
558 271.15 K and under pressure conditions around 2.5 MPa. Figure 11b shows the results of  
559 induction time as a function of the driving force. The latter is calculated using the method  
560 reported by Boufares et al. (2018). This method consists of estimating the CO<sub>2</sub> concentration in  
561 the liquid phase at Hydrate-Liquid-Vapor Equilibrium pressure corresponding to the  
562 experimental temperature (the super-saturation). It is interesting to note from Figure 11b that a  
563 slight increase of the driving force does not have a significant influence on induction time. The  
564 latter increases slightly but the vast majority of the data remains in a narrow range.

565 Overall, these results show that water saturation has small effect on induction time. The  
566 discrepancies observed may also be due to the stochastic nature of hydrate nucleation. However,  
567 given that these findings are based on a limited number of experiences, this analysis should thus  
568 be treated with considerable caution.

### 569 **3.2.2. Effect of particle size**

570 According to literature, pore size is one of the main parameters determining hydrate formation  
571 kinetic in porous media (Borchardt et al., 2016; Nguyen et al., 2020). The results in Table 5  
572 showed that the induction time values at which CO<sub>2</sub> hydrate formation is detected for the 3-

573 particle size classes are relatively homogeneous with an average value of  $87\pm 5$  min. They  
 574 present a difference of  $35\pm 5$  min compared to the induction time obtained for non-sieved silica  
 575 sand as shown on Figure 11b. Overall, it is difficult to establish from these results an obvious  
 576 correlation between induction time and particle size of silica sand. The results reported in the  
 577 literature seem to diverge regarding the effect of particle size on induction time. As observed  
 578 by Qin et al. (2021), some studies demonstrated a positive effect of small particle size on  
 579 shortening the induction time (Heeschen et al., 2016; Zhang et al., 2018). This may be due to a  
 580 larger nucleation area when decreasing particle size. However, other studies found an opposite  
 581 effect even though a similar particle size and porous media were used (Liu et al., 2015; Qin et  
 582 al., 2021). Qin et al. (2021) suggested that the reason for this divergence is related to the fact  
 583 that induction time is strongly affected by many other factors like: (1) the experimental method  
 584 used to form hydrate, (2) the geometry of the experimental device, (3) the type of hydrate  
 585 formed, etc. This could also explain the results obtained in this study.

### 586 3.2.3. Effect of the morphology

587 In this section, results related to the investigation of induction time according to different  
 588 operating conditions: pore size, water saturation of silica gel pore volume and interstitial  
 589 space and driving force were reported in Table 6.

590 Table 6: Operating conditions and results obtained from the experiments of CO<sub>2</sub> hydrate  
 591 formation and dissociation in silica gel

Run	Pore size (nm)	Mass of water injected (g)	Water saturation of Pore volume $S_{wp}$ (%)	Water saturation of Interstitial space $S_{wi}$ (%)	Induction time (min)	Driving force (% mol CO <sub>2</sub> /mol H <sub>2</sub> O)
1	100	5.93	53	0	No hydrate	
2		9.01	78	0	165	0.50
3		11.35	100	0	203	0.80
4		11.01	100	0	102	0.89
5		17.98	100	32	82	0.77
6	30	14.10	100	0	100	0.77
7		19.47	100	30	740	0.92

8		21.83	100	43	253	0.78
---	--	-------	-----	----	-----	------

592 It is well known that the driving force, necessary to initiate the formation of hydrates in silica  
593 gels, increases when the pore sizes decrease because the thermodynamic equilibrium conditions  
594 are more difficult to reach. Therefore, at constant driving force, when the pore sizes decrease  
595 the induction time must increase. This can be seen in Figure 11b where for a driving force  
596 around 0.8 %mol CO<sub>2</sub>/molH<sub>2</sub>O, the induction time increases up to 25 % in 30 nm silica gels  
597 compared to 100 nm. Figure 12 gathers the result obtained for silica gel and silica sand as a  
598 function of the initial water content introduced in the porous media. It can be seen that induction  
599 time values for the experiments performed in silica gel are quite scattered between 82 and  
600 235 min. A significant difference in the induction times was noted in the case of silica gel with  
601 an internal pore size of 30 nm, and a water saturation of the pore volume and the interstitial  
602 space (Run 7, ≈740 min). In addition, it can notice that for a similar initial water content, the  
603 induction time values obtained for silica gel are close, and slightly higher in some cases, than  
604 those obtained in Fontainebleau silica sand. For high water content, particularly in the case of  
605 30 nm pore (Run 7 and 8) size silica gel, the induction time values are higher than in the case  
606 of low water content (Run 6). Knowing that for these two particular experiments, water  
607 occupies both the pore volume and the interstitial space, this points to the hypothesis that water-  
608 gas contact is hindered by the presence of water in the interstitial space.

609 Consequently, it is difficult to draw conclusions, given that hydrate nucleation is a stochastic  
610 process. Furthermore, when water saturates partially the pore volume ( $S_{wp} = 53\%$ ) which  
611 corresponds to an initial water content of 0.37 (correspond to an initial water mass of 6 g) (Run  
612 1), gas hydrate formation was not detected (no DTA signal related to hydrate formation, and no  
613 pressure and temperature variation). This may be due to the adsorption of water on the internal  
614 pore surface of silica gel, which makes the amount of free water not sufficient for hydrate  
615 formation.

#### 616 4. Conclusion

617 In an effort to provide new insights on the influence of key factors related to the use of porous  
618 media on CO<sub>2</sub> hydrates formation and dissociation processes, with a differential thermal  
619 analysis (DTA) approach, the effect of water saturation, particle size and the morphology of the  
620 porous media on induction time, storage capacity and equilibrium conditions on the solid mass  
621 fraction formed and the induction time was investigated:

- 622 • First, water distribution in a silica sand sample was investigated using X-ray micro-  
623 tomography. The analysis of two volume portions taken from the total volume of the  
624 30 %-water saturated silica sand sample allows us to reasonably state that the sample  
625 preparation method used in this study provides a rather homogeneous distribution of  
626 water over the total sample volume.
- 627 • For water saturation, the analysis of the results obtained with silica sand did not reveal  
628 a noteworthy effect on the induction time. Furthermore, when water saturation increases  
629 in a closed system and for the same initial pressure condition, the amount of CO<sub>2</sub>  
630 initially injected in the cell decreases, which results in a lower mass of hydrates formed,  
631 and thus, a lower water to hydrate conversion rates.
- 632 • For particle size, within silica sand, it has shown that this factor does not influence the  
633 induction time, whereas, the results indicated a strong effect on the amount of hydrate  
634 formed. Indeed, for a smaller particle size, liquid-gas contact area is enhanced due to  
635 water adsorption on a larger surface area. This can potentially enhance the amount of  
636 hydrate formed.
- 637 • Finally, this study investigated the influence of the morphology of the porous medium  
638 on hydrate formation and dissociation by using silica sand and spherical dual porous  
639 silica gel. Overall, the results showed a higher amount of thermal energy stored by  
640 hydrates formed in silica gel compared to Fontainebleau silica sand. Moreover, a

641 configuration where water occupies only the pore volume of silica gel was found to be  
642 optimal. In addition, an inhibiting effect on the thermodynamic condition of hydrate  
643 stability was observed. It is well known in the literature that this effect becomes much  
644 more significant as pore size of silica gel particles decreases.

645 **These results showed relatively clear correlations between the factors studied and the fraction**  
646 **of hydrates formed. However, the influence of these factors on the induction time is not obvious.**  
647 **This may be due to coupling problems between these different factors, but also to the lack of**  
648 **information on other factors such as wettability, which would deserve to be studied in depth.**

649 Due to the complexity of the characterization of gas hydrates induction time and the stochastic  
650 nature of hydrate nucleation, this study **also** requires a detailed statistical analysis with several  
651 replicate experiments. Overall, these findings add to a growing body of literature on the link  
652 between hydrate formation and dissociation process and the key factors related to the porous  
653 media. Despite this, **the** calorimetry work carried out in this study could be the basis for further  
654 sets of experiments in order to clearly identify optimal conditions for energy efficient CO<sub>2</sub>  
655 hydrate-based technologies such as cold storage systems.

### 656 **CRedit authorship contribution statement**

657 **Fatima Doria Benmesbah:** Methodology, Software, Investigation, Data curation, Writing –  
658 original draft, Visualization. **Pascal Clain:** Supervision, Validation, Visualization, Writing -  
659 review & editing. **Olivia Fandino:** Supervision. **Veronique Osswald:** Validation,  
660 Visualization. **Laurence Fournaison:** Supervision, **Christophe Dicharry:** Resources,  
661 Methodology, Writing - review & editing. **Livio Ruffine:** Project administration, Resources,  
662 Supervision, Validation, Writing - review & editing. **Anthony Delahaye:** Project  
663 administration, Supervision, Validation, Visualization, Writing - review & editing.

664

## 665 Declaration of Competing Interest

666 The authors declare that they have no known competing financial interests or personal  
667 relationships that could have appeared to influence the work reported in this paper.

## 668 Acknowledgment

669 The authors would like to thank Fatou-Toutie Ndoye and Graciela Alvarez Leguizamo,  
670 researchers at Université Paris-Saclay, FRISE, INRAE, for their technical support, advice and  
671 guidance with the X-ray microtomography device. We are also grateful to Elyamin Dahmana,  
672 for his direct technical help on CO<sub>2</sub> hydrates formation and dissociation experiments using the  
673 DTA device. The authors also acknowledge anonymous reviewers for their valuable  
674 suggestions and remarks.

## 675 5. References

- 676 Adeyemo, A., Kumar, R., Linga, P., Ripmeester, J., Englezos, P., 2010. Capture of carbon dioxide from  
677 flue or fuel gas mixtures by clathrate crystallization in a silica gel column. *International Journal of*  
678 *Greenhouse Gas Control* 4, 478-485.
- 679 Akbari, H., Mertol, A., 1989. Thermal Energy Storage for Cooling of Commercial Buildings, in: Kilkis, B.,  
680 Kakaç, S. (Eds.), *Energy Storage Systems*. Springer Netherlands, Dordrecht, pp. 315–347.
- 681 Anderson, G.K., 2003. Enthalpy of dissociation and hydration number of carbon dioxide hydrate from  
682 the Clapeyron equation. *The Journal of Chemical Thermodynamics* 35, 1171-1183.
- 683 Babu, P., Kumar, R., Linga, P., 2013. Medium pressure hydrate based gas separation (HBGS) process  
684 for pre-combustion capture of carbon dioxide employing a novel fixed bed reactor. *International*  
685 *Journal of Greenhouse Gas Control* 17, 206-214.
- 686 Bagherzadeh, S.A., Moudrakovski, I.L., Ripmeester, J.A., Englezos, P., 2011. Magnetic Resonance  
687 Imaging of Gas Hydrate Formation in a Bed of Silica Sand Particles. *Energy & Fuels* 25, 3083-3092.
- 688 Bhattacharjee, G., Kumar, A., Sakpal, T., Kumar, R., 2015. Carbon Dioxide Sequestration: Influence of  
689 Porous Media on Hydrate Formation Kinetics. *ACS Sustainable Chemistry & Engineering* 3, 1205-1214.
- 690 Bishnoi, P.R., Natarajan, V., 1996. Formation and decomposition of gas hydrates. *Fluid Phase Equilibria*  
691 117, 168-177.
- 692 Borchardt, L., Nickel, W., Casco, M., Senkovska, I., Bon, V., Wallacher, D., Grimm, N., Krause, S.,  
693 Silvestre-Albero, J., 2016. Illuminating solid gas storage in confined spaces – methane hydrate  
694 formation in porous model carbons. *Physical Chemistry Chemical Physics* 18, 20607-20614.
- 695 Boufares, A., Provost, E., Dalmazzone, D., Osswald, V., Clain, P., Delahaye, A., Fournaison, L., 2018.  
696 Kinetic study of CO<sub>2</sub> hydrates crystallization: Characterization using FTIR/ATR spectroscopy and  
697 contribution modeling of equilibrium/non-equilibrium phase-behavior. *Chemical Engineering Science*  
698 192, 371-379.
- 699 Chami, N., Bendjenni, S., Clain, P., Osswald, V., Delahaye, A., Fournaison, L., Dalmazzone, D., 2021.  
700 Thermodynamic characterization of mixed gas hydrates in the presence of cyclopentane as guest  
701 molecule for an application in secondary refrigeration. *Chemical Engineering Science* 244, 116790.
- 702 Cheng, C., Wang, F., Tian, Y., Wu, X., Zheng, J., Zhang, J., Li, L., Yang, P., Zhao, J., 2020. Review and  
703 prospects of hydrate cold storage technology. *Renewable and Sustainable Energy Reviews* 117,  
704 109492.

- 705 Chong, Z.R., Yang, M., Khoo, B.C., Linga, P., 2016. Size Effect of Porous Media on Methane Hydrate  
706 Formation and Dissociation in an Excess Gas Environment. *Industrial & Engineering Chemistry*  
707 *Research* 55, 7981-7991.
- 708 Clain, P., 2014. Couplage entre le stockage et distribution de froid par coulis d'hydrates. Sorbonne  
709 Université, Paris.
- 710 Dai, S., Lee, J.Y., Santamarina, J.C., 2014. Hydrate nucleation in quiescent and dynamic conditions. *Fluid*  
711 *Phase Equilibria* 378, 107-112.
- 712 Darbouret, M., Cournil, M., Herri, J.-M., 2005. Rheological study of TBAB hydrate slurries as secondary  
713 two-phase refrigerants. *International Journal of Refrigeration* 28, 663-671.
- 714 Davies, S.R., Hester, K.C., Lachance, J.W., Koh, C.A., Dendy Sloan, E., 2009. Studies of hydrate  
715 nucleation with high pressure differential scanning calorimetry. *Chemical Engineering Science* 64, 370-  
716 375.
- 717 Delahaye, A., Fournaison, L., Dalmazzone, D., 2018. Use of Hydrates for Cold Storage and Distribution  
718 in Refrigeration and Air-Conditioning Applications, *Gas Hydrates 2*. John Wiley & Sons, Ltd, pp. 315-  
719 358.
- 720 Delahaye, A., Fournaison, L., Marinha, S., Martínez, M.C., 2008. Rheological study of CO<sub>2</sub> hydrate  
721 slurry in a dynamic loop applied to secondary refrigeration. *Chemical Engineering Science* 63, 3551-  
722 3559.
- 723 Dicharry, C., Duchateau, C., Asbaï, H., Broseta, D., Torrè, J.-P., 2013. Carbon dioxide gas hydrate  
724 crystallization in porous silica gel particles partially saturated with a surfactant solution. *Chemical*  
725 *Engineering Science* 98, 88-97.
- 726 Dufour, T., Hoang, H.M., Oignet, J., Osswald, V., Clain, P., Fournaison, L., Delahaye, A., 2017. Impact of  
727 pressure on the dynamic behavior of CO<sub>2</sub> hydrate slurry in a stirred tank reactor applied to cold  
728 thermal energy storage. *Applied Energy* 204, 641-652.
- 729 Englezos, P., 1993. Clathrate hydrates. *Industrial & Engineering Chemistry Research* 32, 1251-1274.
- 730 Englezos, P., Kalogerakis, N., Dholabhai, P.D., Bishnoi, P.R., 1987. Kinetics of formation of methane and  
731 ethane gas hydrates. *Chemical Engineering Science* 42, 2647-2658.
- 732 Fitzgerald, G.C., Castaldi, M.J., Schicks, J.M., 2014. Methane Hydrate Formation and Thermal Based  
733 Dissociation Behavior in Silica Glass Bead Porous Media. *Industrial & Engineering Chemistry Research*  
734 53, 6840-6854.
- 735 Fournaison, L., Delahaye, A., Chatti, I., Petitet, J.-P., 2004. CO<sub>2</sub> Hydrates in Refrigeration Processes.  
736 *Industrial & Engineering Chemistry Research* 43, 6521-6526.
- 737 Ge, B.-B., Zhong, D.-L., Lu, Y.-Y., 2019. Influence of water saturation and particle size on methane  
738 hydrate formation and dissociation in a fixed bed of silica sand. *Energy Procedia* 158, 5402-5407.
- 739 Gupta, A., Lachance, J., Sloan, E.D., Koh, C.A., 2008. Measurements of methane hydrate heat of  
740 dissociation using high pressure differential scanning calorimetry. *Chemical Engineering Science* 63,  
741 5848-5853.
- 742 Handa, Y.P., Stupin, D.Y., 1992. Thermodynamic properties and dissociation characteristics of methane  
743 and propane hydrates in 70-Å-radius silica gel pores. *The Journal of Physical Chemistry* 96, 8599-  
744 8603.
- 745 Hasnain, S.M., 1998. Review on sustainable thermal energy storage technologies, Part II: cool thermal  
746 storage. *Energy Conversion and Management* 39, 1139-1153.
- 747 Heeschen, K.U., Schicks, J.M., Oeltzschner, G., 2016. The promoting effect of natural sand on methane  
748 hydrate formation: Grain sizes and mineral composition. *Fuel* 181, 139-147.
- 749 Jerbi, S., Delahaye, A., Fournaison, L., Haberschill, P., 2010. Characterization of CO<sub>2</sub> hydrate formation  
750 and dissociation kinetics in a flow loop. *International Journal of Refrigeration* 33, 1625-1631.
- 751 Joshi, A., Sangwai, J.S., Das, K., Sami, N.A., 2013. Experimental investigations on the phase equilibrium  
752 of semiclathrate hydrates of carbon dioxide in TBAB with small amount of surfactant. *International*  
753 *Journal of Energy and Environmental Engineering* 4, 11.
- 754 Kang, S.-P., Lee, H., Ryu, B.J., 2001. Enthalpies of dissociation of clathrate hydrates of carbon dioxide,  
755 nitrogen, (carbon dioxide + nitrogen), and (carbon dioxide + nitrogen + tetrahydrofuran). *The Journal*  
756 *of Chemical Thermodynamics* 33, 513-521.



- 757 Kang, S.-P., Lee, J.-W., Ryu, H.-J., 2008. Phase behavior of methane and carbon dioxide hydrates in  
758 meso- and macro-sized porous media. *Fluid Phase Equilibria* 274, 68-72.
- 759 Kang, S.-P., Lee, J., Seo, Y., 2013. Pre-combustion capture of CO<sub>2</sub> by gas hydrate formation in silica gel  
760 pore structure. *Chemical Engineering Journal* 218, 126-132.
- 761 Kashchiev, D., Firoozabadi, A., 2002. Nucleation of gas hydrates. *Journal of Crystal Growth* 243, 476-  
762 489.
- 763 Kumar, A., Khatri, D., Lee, J.D., Kumar, R., 2016. Crystallization kinetics for carbon dioxide gas hydrate  
764 in fixed bed and stirred tank reactor. *Korean Journal of Chemical Engineering* 33, 1922-1930.
- 765 Kumar, A., Sakpal, T., Linga, P., Kumar, R., 2013. Influence of contact medium and surfactants on carbon  
766 dioxide clathrate hydrate kinetics. *Fuel* 105, 664-671.
- 767 Kumar, A., Sakpal, T., Roy, S., Kumar, R., 2015. Methane hydrate formation in a test sediment of sand  
768 and clay at various levels of water saturation. *Canadian Journal of Chemistry* 93, 874-881.
- 769 Laugier, F., Andriantsiferana, C., Wilhelm, A.M., Delmas, H., 2008. Ultrasound in gas-liquid systems:  
770 Effects on solubility and mass transfer. *Ultrasonics Sonochemistry* 15, 965-972.
- 771 Lee, K., Lee, S.-H., Lee, W., 2013. Stochastic nature of carbon dioxide hydrate induction times in Na-  
772 montmorillonite and marine sediment suspensions. *International Journal of Greenhouse Gas Control*  
773 14, 15-24.
- 774 Li, G., Hwang, Y., Radermacher, R., 2012. Review of cold storage materials for air conditioning  
775 application. *International Journal of Refrigeration* 35, 2053-2077.
- 776 Lievois, J.S., Perkins, R., Martin, R.J., Kobayashi, R., 1990. Development of an automated, high pressure  
777 heat flux calorimeter and its application to measure the heat of dissociation and hydrate numbers of  
778 methane hydrate. *Fluid Phase Equilibria* 59, 73-97.
- 779 Lin, W., Dalmazzone, D., Fürst, W., Delahaye, A., Fournaison, L., Clain, P., 2014. Thermodynamic  
780 properties of semiclathrate hydrates formed from the TBAB+TBPB+water and CO<sub>2</sub>+TBAB+TBPB+water  
781 systems. *Fluid Phase Equilibria* 372, 63-68.
- 782 Linga, P., Clarke, M.A., 2017. A Review of Reactor Designs and Materials Employed for Increasing the  
783 Rate of Gas Hydrate Formation. *Energy & Fuels* 31, 1-13.
- 784 Linga, P., Daraboina, N., Ripmeester, J.A., Englezos, P., 2012. Enhanced rate of gas hydrate formation  
785 in a fixed bed column filled with sand compared to a stirred vessel. *Chemical Engineering Science* 68,  
786 617-623.
- 787 Linga, P., Haligva, C., Nam, S.C., Ripmeester, J.A., Englezos, P., 2009. Gas Hydrate Formation in a  
788 Variable Volume Bed of Silica Sand Particles. *Energy & Fuels* 23, 5496-5507.
- 789 Linga, P., Kumar, R., Lee, J.D., Ripmeester, J., Englezos, P., 2010. A new apparatus to enhance the rate  
790 of gas hydrate formation: Application to capture of carbon dioxide. *International Journal of*  
791 *Greenhouse Gas Control* 4, 630-637.
- 792 Liu, W., Wang, S., Yang, M., Song, Y., Wang, S., Zhao, J., 2015. Investigation of the induction time for  
793 THF hydrate formation in porous media. *Journal of Natural Gas Science and Engineering* 24, 357-364.
- 794 Loveday, J.S., Nelmes, R.J., 2008. High-pressure gas hydrates. *Phys. Chem. Chem. Phys.* 10, 937-950.
- 795 Lu, H., Kawasaki, T., Ukita, T., Moudrakovski, I., Fujii, T., Noguchi, S., Shimada, T., Nakamizu, M.,  
796 Ripmeester, J., Ratcliffe, C., 2011. Particle size effect on the saturation of methane hydrate in  
797 sediments – Constrained from experimental results. *Marine and Petroleum Geology* 28, 1801-1805.
- 798 Malagar, B.R.C., Lijith, K.P., Singh, D.N., 2019. Formation & dissociation of methane gas hydrates in  
799 sediments: A critical review. *Journal of Natural Gas Science and Engineering* 65, 168-184.
- 800 Marinha, S., Delahaye, A., Fournaison, L., 2007. Solid fraction modelling for CO<sub>2</sub> and CO<sub>2</sub>-THF hydrate  
801 slurries used as secondary refrigerants. *International Journal of Refrigeration* 30, 758-766.
- 802 Martínez, M.C., Dalmazzone, D., Fürst, W., Delahaye, A., Fournaison, L., 2008. Thermodynamic  
803 properties of THF + CO<sub>2</sub> hydrates in relation with refrigeration applications. *AIChE Journal* 54, 1088-  
804 1095.
- 805 Mekala, P., Busch, M., Mech, D., Patel, R.S., Sangwai, J.S., 2014. Effect of silica sand size on the  
806 formation kinetics of CO<sub>2</sub> hydrate in porous media in the presence of pure water and seawater  
807 relevant for CO<sub>2</sub> sequestration. *Journal of Petroleum Science and Engineering* 122, 1-9.

- 808 Natarajan, V., Bishnoi, P.R., Kalogerakis, N., 1994. Induction phenomena in gas hydrate nucleation.  
809 Chemical Engineering Science 49, 2075-2087.
- 810 Nguyen, N.N., Galib, M., Nguyen, A.V., 2020. Critical Review on Gas Hydrate Formation at Solid Surfaces  
811 and in Confined Spaces—Why and How Does Interfacial Regime Matter? Energy & Fuels 34, 6751-6760.
- 812 Oya, S., Aifaa, M., Ohmura, R., 2017. Formation, growth and sintering of CO<sub>2</sub> hydrate crystals in liquid  
813 water with continuous CO<sub>2</sub> supply: Implication for subsurface CO<sub>2</sub> sequestration. International Journal  
814 of Greenhouse Gas Control 63, 386-391.
- 815 Pan, Z., Liu, Z., Zhang, Z., Shang, L., Ma, S., 2018. Effect of silica sand size and saturation on methane  
816 hydrate formation in the presence of SDS. Journal of Natural Gas Science and Engineering 56, 266-280.
- 817 Park, J., Seo, Y.-T., Lee, J.-w., Lee, H., 2006. Spectroscopic analysis of carbon dioxide and nitrogen mixed  
818 gas hydrates in silica gel for CO<sub>2</sub> separation. Catalysis Today 115, 279-282.
- 819 Prah, B., Yun, R., 2018. CO<sub>2</sub> hydrate slurry transportation in carbon capture and storage. Applied  
820 Thermal Engineering 128, 653-661.
- 821 Qin, Y., Bao, R., Shang, L., Zhou, L., Meng, L., Zang, C., Sun, X., 2022. Effects of Particle Size and Types  
822 of Porous Media on the Formation and Occurrence of Methane Hydrate in Complex Systems. Energy  
823 & Fuels 36, 655-668.
- 824 Qin, Y., Pan, Z., Liu, Z., Shang, L., Zhou, L., 2021. Influence of the Particle Size of Porous Media on the  
825 Formation of Natural Gas Hydrate: A Review. Energy & Fuels 35, 11640-11664.
- 826 Rehman, A.N., Lal, B., Pendyala, R., Yusoff, M.H.M., 2022. Unusual CO<sub>2</sub> hydrate formation in porous  
827 media: Implications on geo-CO<sub>2</sub> storage laboratory testing methods. Materials Today: Proceedings 57,  
828 1363-1368.
- 829 Sahu, C., Sircar, A., Sangwai, J.S., Kumar, R., 2022. Effect of sodium tripolyphosphate (STPP) and  
830 tetrasodium pyrophosphate (TSP) on the formation kinetics of CO<sub>2</sub> hydrate in bulk and porous media  
831 in the presence of pure water and seawater relevant for CO<sub>2</sub> sequestration. International Journal of  
832 Greenhouse Gas Control 114, 103564.
- 833 Shindo, Y., Lund, P.C., Fujioka, Y., Komiyama, H., 1993. Kinetics and mechanism of the formation of  
834 CO<sub>2</sub> hydrate. International Journal of Chemical Kinetics 25, 777-782.
- 835 Skovborg, P., Ng, H.J., Rasmussen, P., Mohn, U., 1993. Measurement of induction times for the  
836 formation of methane and ethane gas hydrates. Chemical Engineering Science 48, 445-453.
- 837 Sloan, E.D., 1998. Physical/chemical properties of gas hydrates and application to world margin  
838 stability and climatic change. Geological Society, London, Special Publications 137, 31-50.
- 839 Sloan, E.D., Fleyfel, F., 1992. Hydrate dissociation enthalpy and guest size. Fluid Phase Equilibria 76,  
840 123-140.
- 841 Sloan, E.D., Koh, C.A., 2007. Clathrate Hydrates of Natural Gases, 3rd edition ed. CRC Press, Boca Raton.
- 842 Smith, D.H., Wilder, J.W., Seshadri, K., 2002. Thermodynamics of Carbon Dioxide Hydrate Formation in  
843 Media with Broad Pore-Size Distributions. Environmental Science & Technology 36, 5192-5198.
- 844 Torr , J.-P., Dicharry, C., Ricaurte, M., Daniel-David, D., Broseta, D., 2011. CO<sub>2</sub> capture by hydrate  
845 formation in quiescent conditions: In search of efficient kinetic additives. Energy Procedia 4, 621-628.
- 846 Turner, D.J., Cherry, R.S., Sloan, E.D., 2005. Sensitivity of methane hydrate phase equilibria to sediment  
847 pore size. Fluid Phase Equilibria 228-229, 505-510.
- 848 Uchida, T., Ebinuma, T., Takeya, S., Nagao, J., Narita, H., 2002. Effects of Pore Sizes on Dissociation  
849 Temperatures and Pressures of Methane, Carbon Dioxide, and Propane Hydrates in Porous Media. The  
850 Journal of Physical Chemistry B 106, 820-826.
- 851 Wang, J., Zhang, L., Ge, K., Dong, H., 2021. Capillary pressure in the anisotropy of sediments with  
852 hydrate formation. Fuel 289, 119938.
- 853 Wang, X., Dennis, M., 2017. Thermal energy harvest in the discharge of CO<sub>2</sub> semi-clathrate hydrate in  
854 an emulated cold storage system. Applied Thermal Engineering 124, 725-733.
- 855 Wang, X., Dennis, M., Hou, L., 2014. Clathrate hydrate technology for cold storage in air conditioning  
856 systems. Renewable and Sustainable Energy Reviews 36, 34-51.
- 857 Wang, X., Zhang, F., Lipiński, W., 2020. Carbon dioxide hydrates for cold thermal energy storage: A  
858 review. Solar Energy 211, 11-30.

- 859 Wang, Z., Li, F., Fan, T., Xiong, W., Yang, B., 2015. Research on the Application of Gas Hydrate in Cool  
 860 Storage Air Conditioning. *Procedia Engineering* 121, 1118-1125.
- 861 Yang, M., Song, Y., Jiang, L., Liu, Y., Wang, X., 2015. Behaviour of hydrate-based technology for H<sub>2</sub>/CO<sub>2</sub>  
 862 separation in glass beads. *Separation and Purification Technology* 141, 170-178.
- 863 Yang, M., Song, Y., Ruan, X., Liu, Y., Zhao, J., Li, Q., 2012. Characteristics of CO<sub>2</sub> Hydrate Formation and  
 864 Dissociation in Glass Beads and Silica Gel. *Energies* 5, 925-937.
- 865 Zhang, B., Zhou, L., Liu, C., Zhang, Q., Wu, Q., Wu, Q., Liu, C., 2018. Influence of sediment media with  
 866 different particle sizes on the nucleation of gas hydrate. *Natural Gas Industry B* 5, 652-659.
- 867 Zhang, F., Wang, X., Wang, B., Lou, X., Lipiński, W., 2022. Effects of silica gel nanopores and surfactants  
 868 on CO<sub>2</sub> hydrate formation kinetics—An experimental and modeling study. *Chemical Engineering  
 869 Science* 262, 118002.
- 870 Zhang, X., Li, J., Wu, Q., Wang, C., Nan, J., 2015. Experimental study on the effect of pore size on carbon  
 871 dioxide hydrate formation and storage in porous media. *Journal of Natural Gas Science and  
 872 Engineering* 25, 297-302.
- 873 Zhang, Y., Li, X.-S., Chen, Z.-Y., Li, G., Wang, Y., 2016. Effects of particle and pore sizes on the formation  
 874 behaviors of methane hydrate in porous silica gels. *Journal of Natural Gas Science and Engineering* 35,  
 875 1463-1471.
- 876 Zhang, Y., Li, X., Chen, Z., Xia, Z., Wang, Y., Li, G., 2017. Formation Behavior and Controlling Factor of  
 877 Methane Hydrate in Porous Media. *Energy Procedia* 142, 4044-4049.

878

879 Paris, 13th june 2022

880 *Attention to Editor of Chemical Engineering*  
 881 *Science*

882

883 Dear Madam, Dear Sir,

884

885 Please find in attached file our paper entitled "Calorimetric study of carbon dioxide (CO<sub>2</sub>) hydrate  
 886 formation and dissociation processes in a porous media." by Fatima Doria Benmesbah, Pascal Clain,  
 887 Olivia Fandino Livio Ruffine, Véronique Osswald, Laurence Fournaison, Christophe Dicharry and  
 888 Anthony Delahaye, and for a submission as original article in **Chemical Engineering Science**.

889

890 **Highlights**

- 891 • Calorimetric study of CO<sub>2</sub> hydrates formation and dissociation in silica sand and gel.
- 892 • Induction time of CO<sub>2</sub> hydrates is not influenced by water saturation.
- 893 • Silica sand of particle size of have a great effect on the amount of hydrates formed.
- 894 • Morphology of porous medium used have a big impact on the amount of hydrates formed.
- 895 • Better results have been obtained with silica gel than Fontainebleau sand.

896

897

Best Regards,

898

Fatima Benmesbah

899

900 Keywords: CO<sub>2</sub> hydrate, Cold storage, Differential thermal analysis, Particle and Pore size, Porous  
 901 media, Water saturation

902

903 Corresponding authors:

904 Fatima Benmesbah and Pascal Clain

905

906 IFREMER, Département Ressources physiques et Ecosystèmes de fond de Mer (REM), Unité des  
 907 Géosciences Marines, 29280 Plouzané, France.

908

909 Université Paris-Saclay, INRAE, FRISE, 92761, Antony, France

910

911 Tel: 33 (0)1 81 00 28 37 – E-mail : pascal.clain@devinci.fr

912

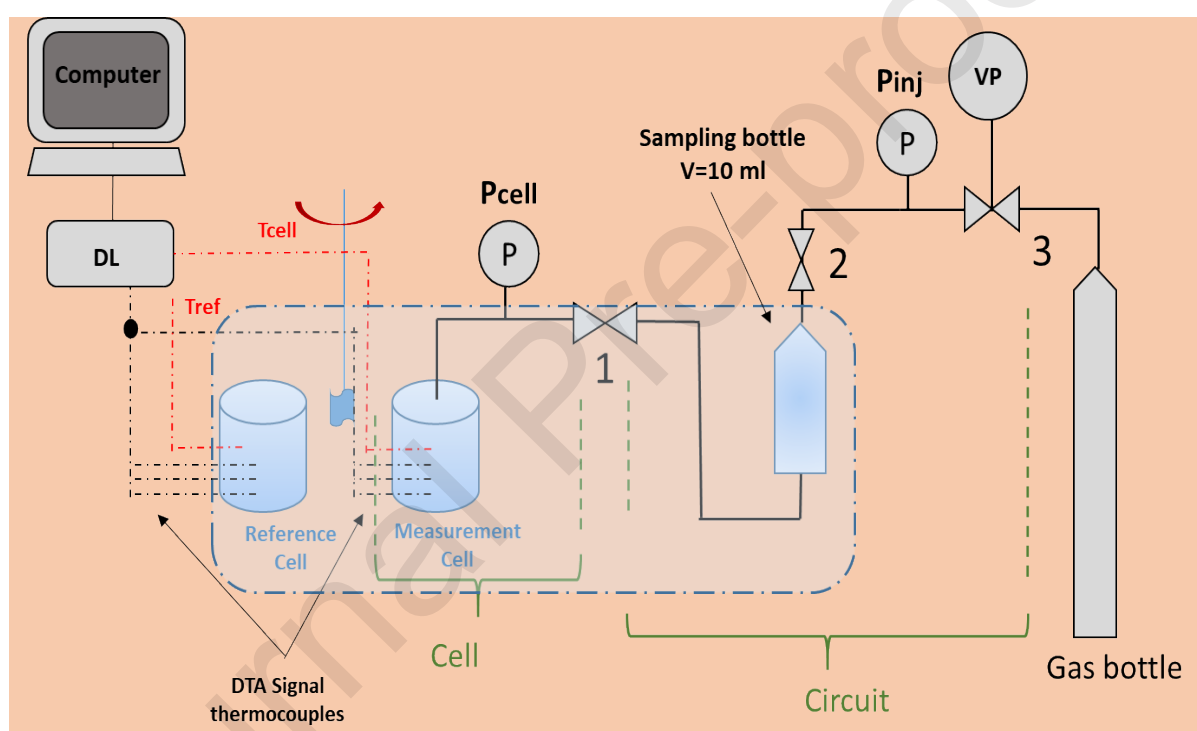
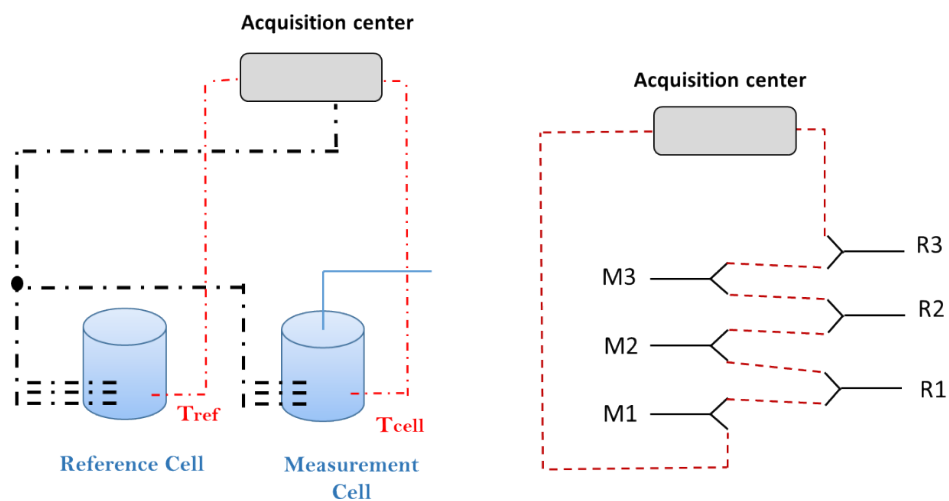


Figure 1: Schematic diagram of the DTA experimental apparatus. (DL) Data logger, (P) Pressure transducer, ( $T_{cell}$ ,  $T_{ref}$ ) Thermocouple to measure direct temperature, (VP) Vacuum pump, the blue area corresponds to a temperature-controlled bath in which the two cells are immersed, as well as the sampling cylinder

913

914



915

916 Figure 2: Diagram of the six thermocouples connected in series to obtain the DTA signal. M1,  
917 M2 and M3 correspond to the thermocouples placed in the measuring cell. R1, R2 and R3  
918 correspond to the thermocouples placed in the reference cell

919

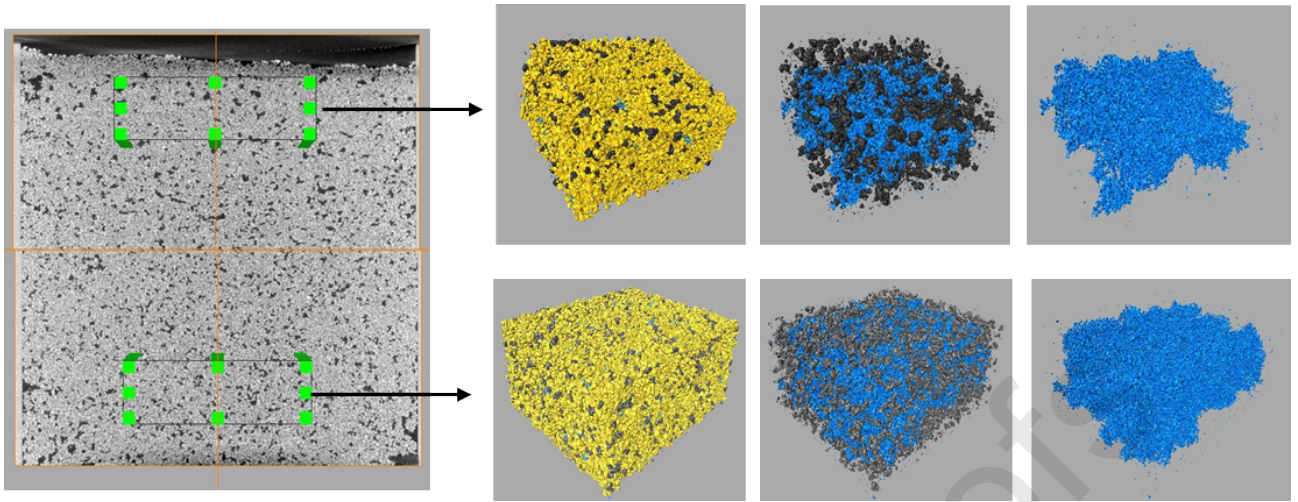
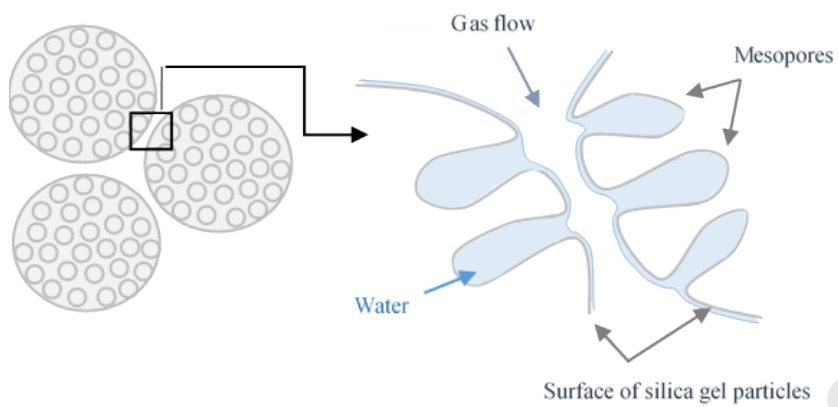


Figure 3: CT scan analysis of a sand sample for a water saturation of 66%. Sand is represented in yellow, water in blue and air in dark grey.

920

921

Journal Pre-proofs



922 Figure 4: Schematic illustration of water occupying the mesoporous volume of silica gel  
923 particles

924

Journal Pre-proofs

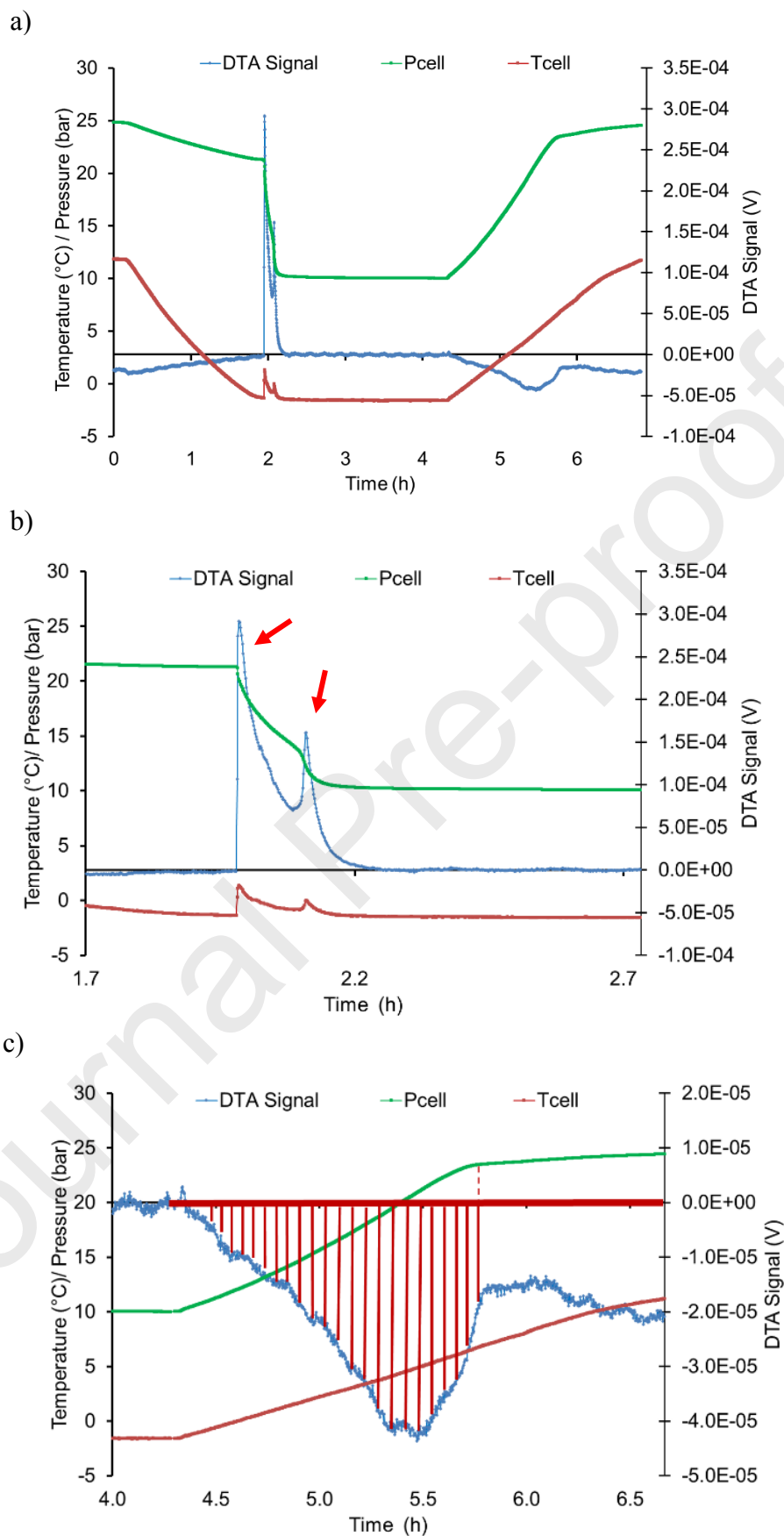


Figure 5: a) Temperature, pressure and DTA signal profiles during CO<sub>2</sub> hydrate formation and dissociation in silica sand at 33 % water



saturation. Figures b) and c) focus on CO<sub>2</sub> hydrates formation peak and CO<sub>2</sub> hydrates dissociation peak respectively.

925

926

Journal Pre-proofs

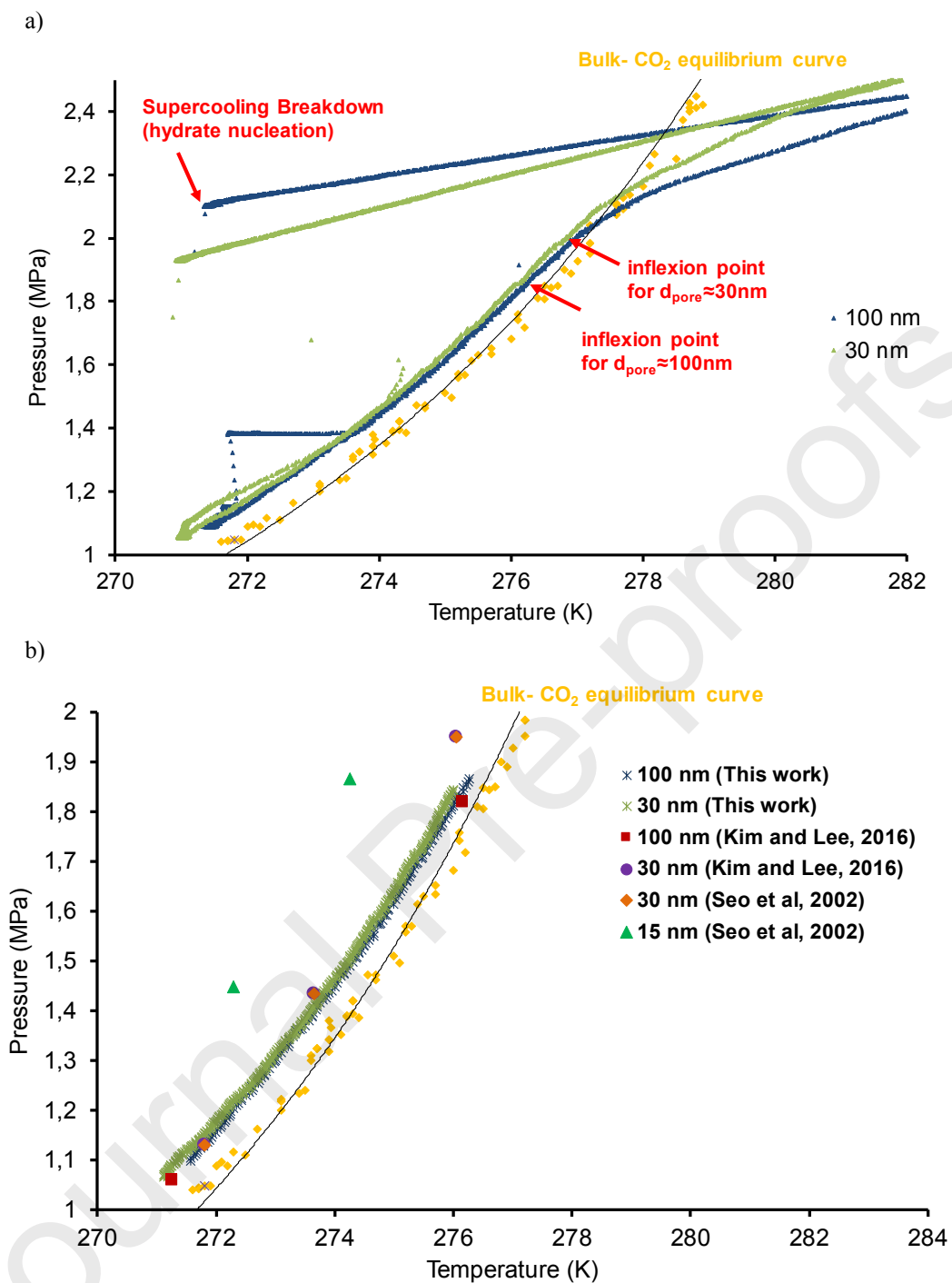


Figure 6: Temperature vs pressure profile of CO<sub>2</sub> gas hydrates in silica gel with several pore sizes. Results of previous studies in the literature are also reported (Kim and Lee, 2016; Seo et al., 2002)

927

928

929

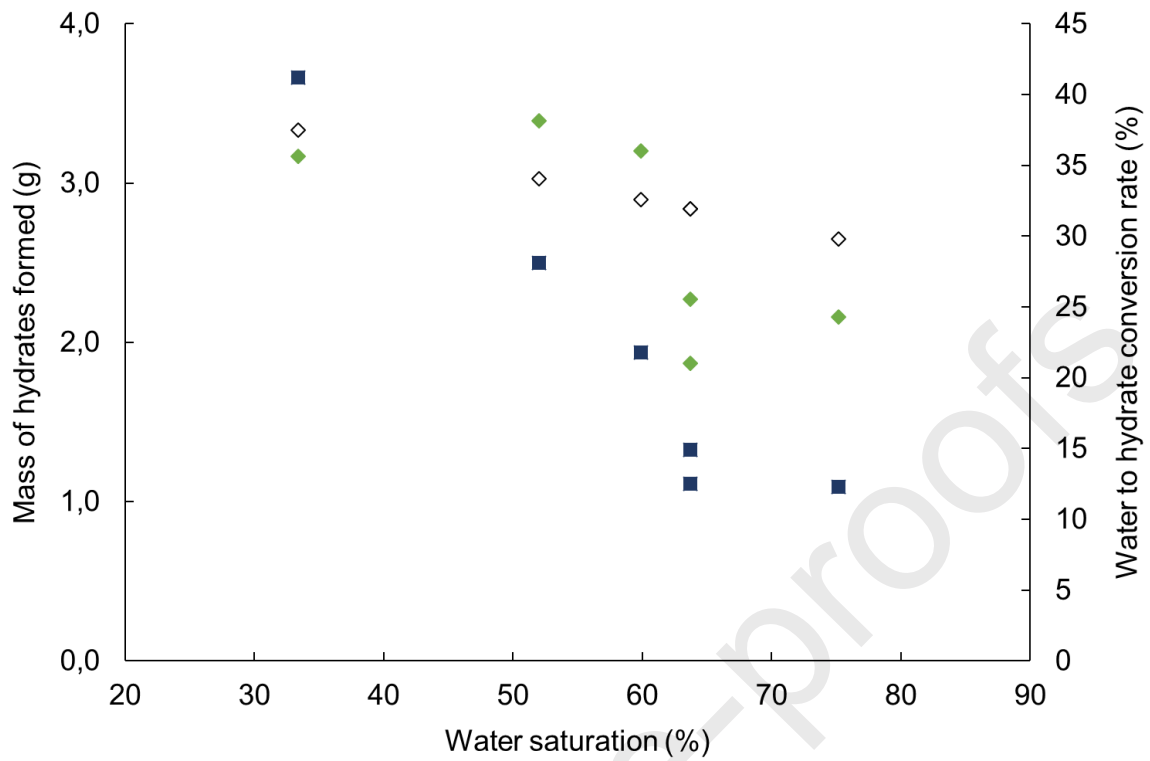


Figure 7: Mass of hydrate formed (◆ : present calorimetric approach; ◇ : previous mass balance approach (Marinhas et al., 2007) and water to hydrate conversion rate (■) as a function of water saturation of silica sand.

930

931

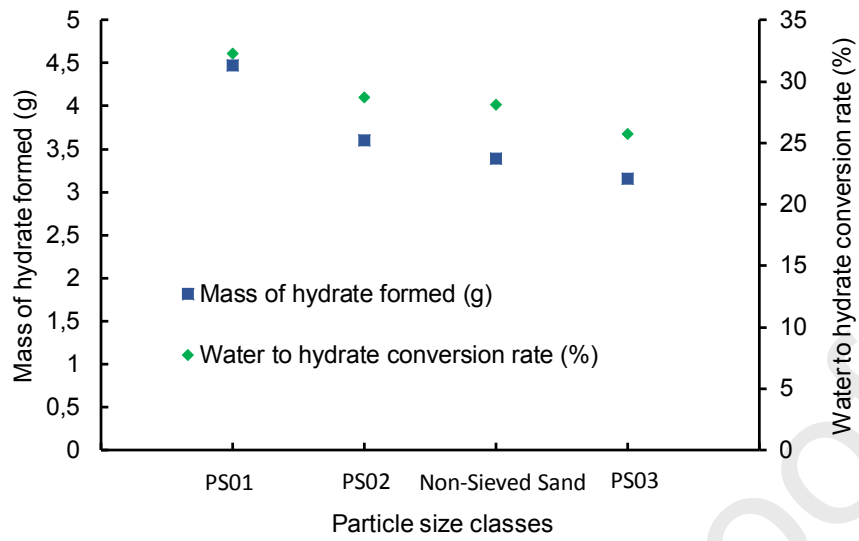


Figure 8: Mass of hydrate formed (◆) and water to hydrate conversion rate (■) as a function of particle size of silica sand.

932

933

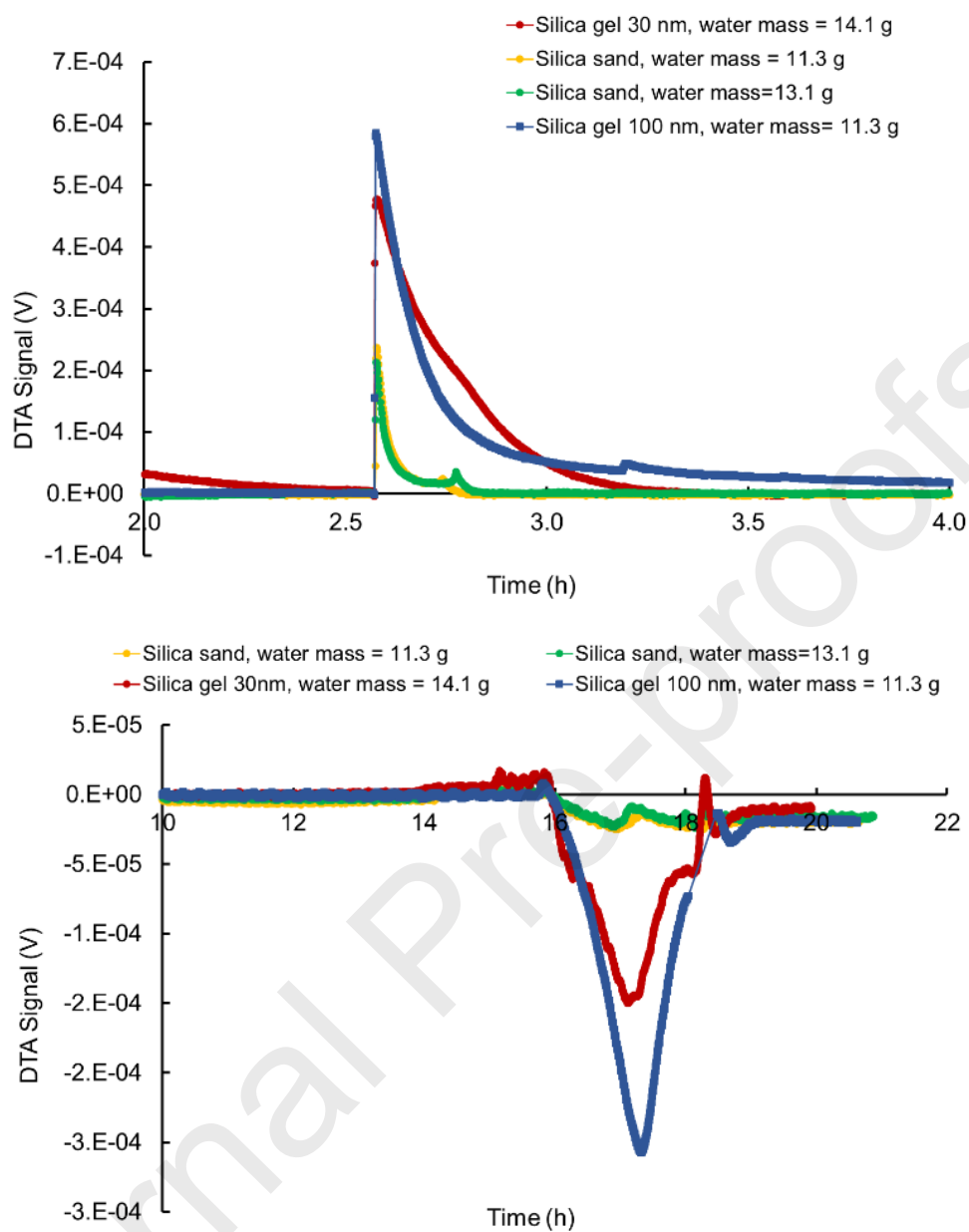


Figure 9: Comparison of DTA signal of CO<sub>2</sub> hydrate formation peaks in silica sand (Run 4 and 6, Table 3), and silica gel (Run 3 and 6, Table 5)

934

935

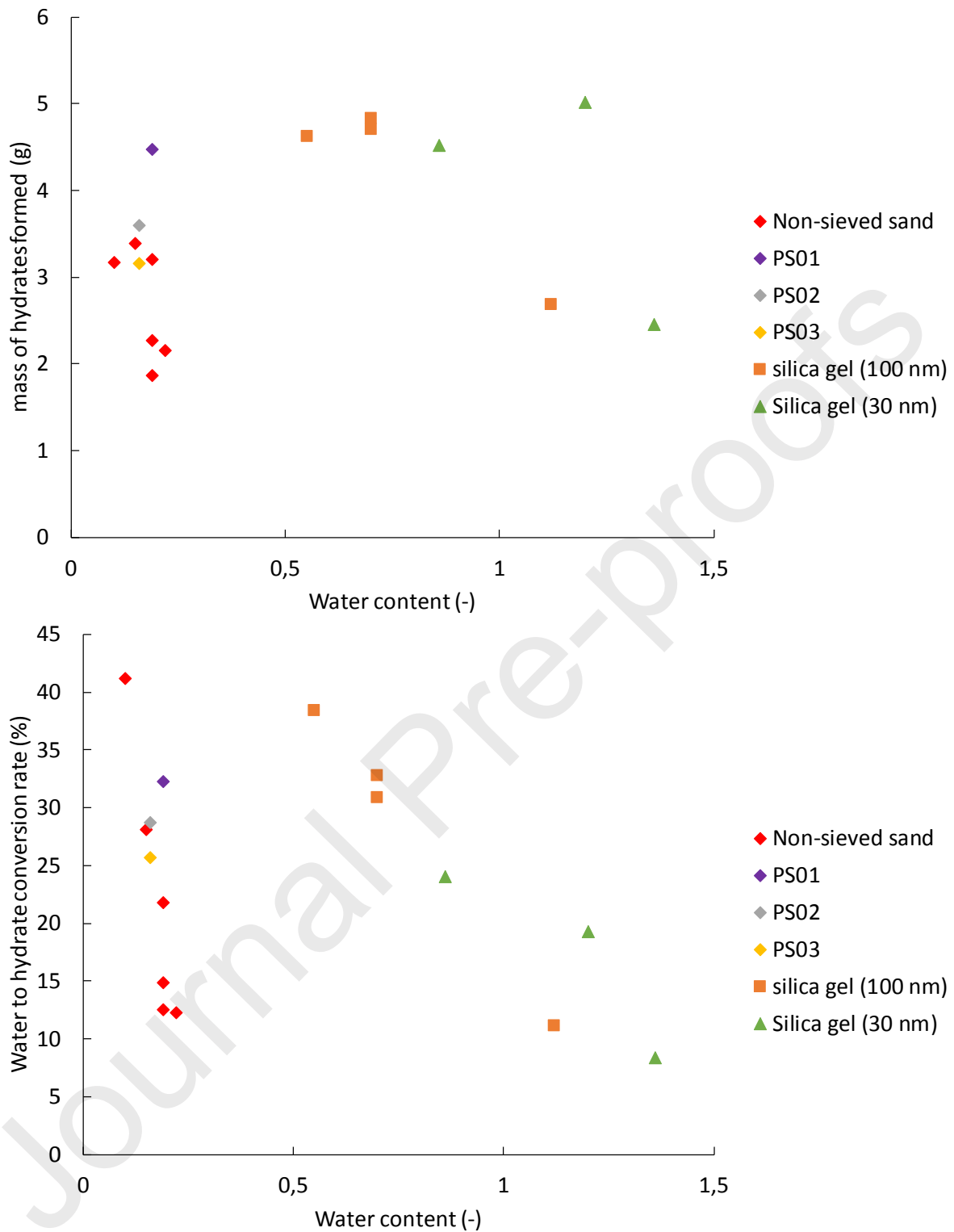


Figure 10: Mass of hydrate formed and water to hydrate conversion rate as a function of initial water content.

936

937

938

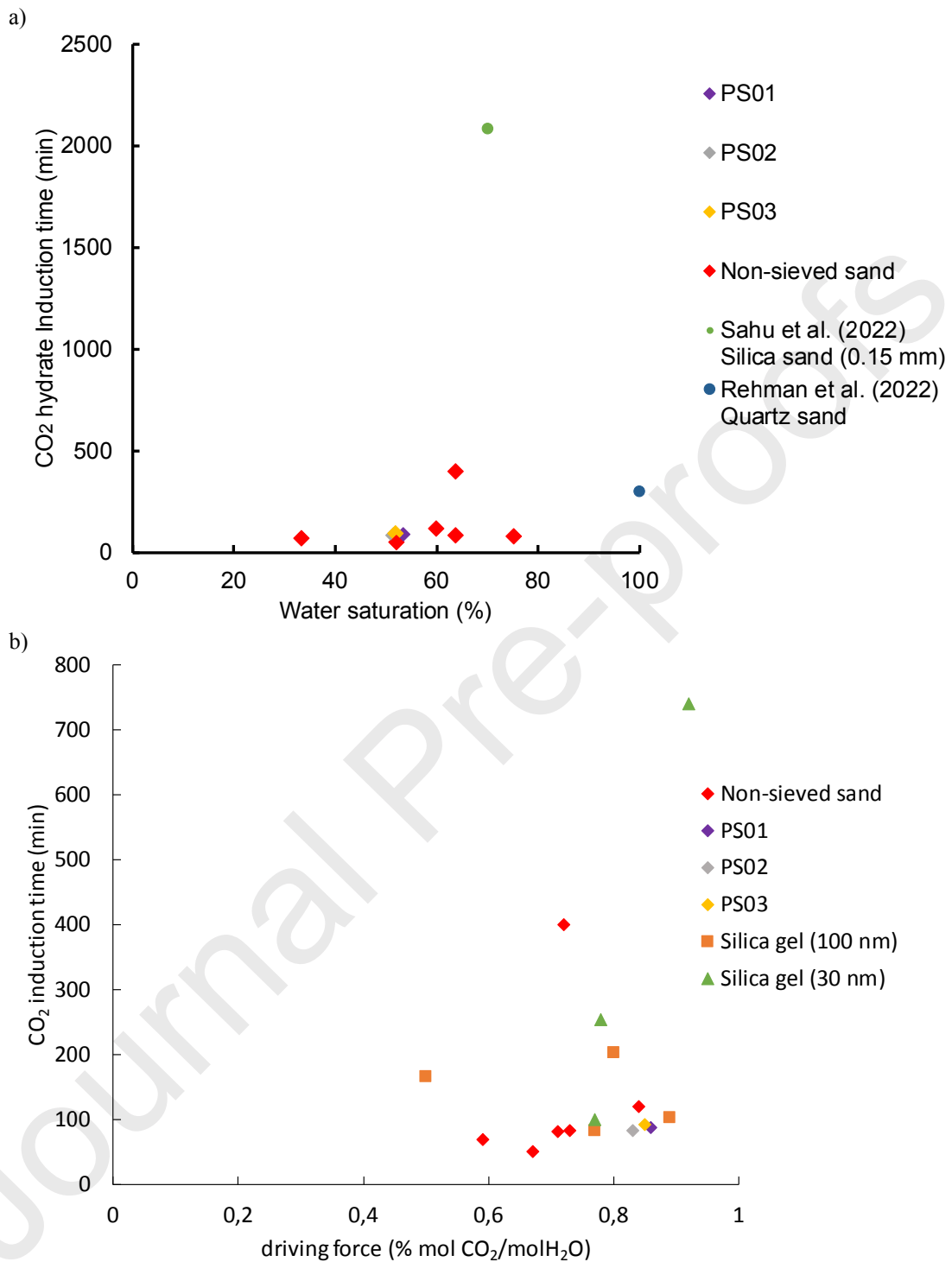


Figure 11: Induction time as a function of a) water saturation of silica sand and particles size, b) the driving force induced by the experimental conditions.

939

940

941

942

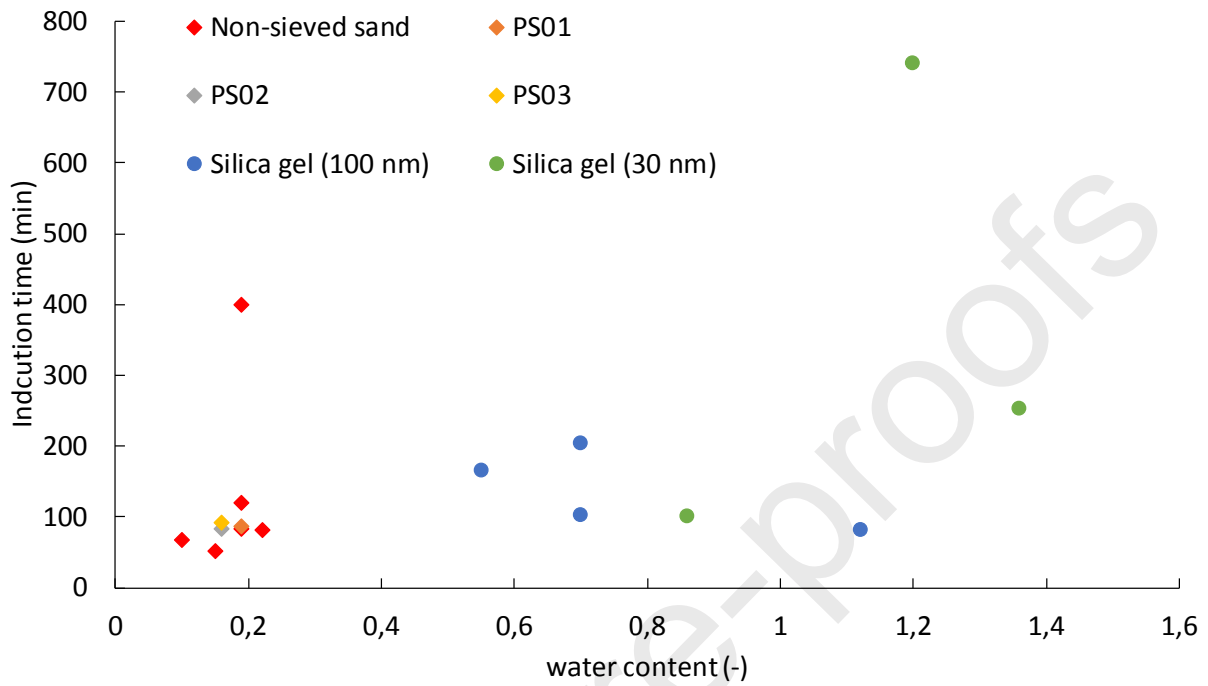


Figure 12: Induction time in silica sand, 100 nm silica gel and 30 nm silica gel as a function of initial water content.

943

944



945

946

Table 4: Physical properties of Fontainebleau silica sand and silica gel samples.

<b>Parameters</b>	<b>Fontainebleau silica sand</b>	<b>30 nm Silica gel</b>	<b>100 nm Silica gel</b>
<b>Mean particle diameter (<math>\mu\text{m}</math>)</b>	80-450	20-45	20-45
<b>Mean pore diameter (nm)</b>	-	30	100
<b>Pore volume (<math>\text{cm}^3.\text{g}^{-1}</math>)</b>	-	0.86	0.7
<b>Dry density (<math>\text{g}.\text{cm}^{-3}</math>)</b>	2.65	2.2	2.2

947

948

949  
950

Table 5: Volume fractions of air, water and packed silica sand within the analyzed volumes by micro-tomography

<b>Analyzed Volume</b>	<b>Material</b>	<b>Volume fraction (%)</b>	<b>Total volume (cm<sup>3</sup>)</b>
<b>Upper part</b>	Air	0.10	0.529
	Water	0.19	
	Silica Sand	0.71	
<b>Lower part</b>	Air	0.10	0.190
	Water	0.19	
	Silica Sand	0.71	

951

952

953  
954Table 6: CO<sub>2</sub> hydrate formation and dissociation results in a sandy matrix for several water saturations and particle size

Run	Sample state*	Particle size (μm)	Water mass (g)	Water saturation (%)	Mass of Solid particles (g)	Water content	Mass of hydrates formed (g)	Water conversion to hydrate (%)
1	F	Non-sieved sand	5.78	33.4	59.58	0.10	3.17	41.2
2	F		9.00	52.0	59.57	0.15	3.39	28.1
3	F		11.05	59.9	56.60	0.19	3.20	21.8
4	F		11.32	63.7	58.37	0.19	1.87	12.5
5	M		11.32	63.7	58.37	0.19	2.27	14.9
6	F		13.10	75.2	59.31	0.22	2.16	12.3
7	F		17.45	100	59.36	0.29	No hydrate formation succeeded	
8	F	PS01	10.34	53.4	54.16	0.19	4.47	32.3
9	F	PS02	9.37	51.5	57.15	0.16	3.60	28.7
10	F	PS03	9.20	51.8	58.36	0.16	3.16	25.7

955  
956  
957

\*F: fresh sample. M: memory sample. In the latter state, Run 5 represents a repeatability test for Run 4 (without changing the sample).

958

Table 4: CO<sub>2</sub> hydrate formation and dissociation results in silica gel

Run	Pore size (nm)	Mass of water injected (g)	Water saturation of Pore volume $Sw_p$ (%)	Water saturation of Interstitial space $Sw_i$ (%)	Mass of solid particles (g)	Water content	Induction time (min)	Mass of hydrate formed (g)	Water to hydrate conversion rate (%)
1	100	5.93	53	0	15.99	0.37	No hydrate		
2		9.01	78	0	16.46	0.55	165	4.63	38.4
3		11.35	100	0	16.22	0.70	203	4.70	30.9
4		11.01	100	0	15.73	0.70	102	4.83	32.8
5		17.98	100	32	16.00	1.12	82	2.68	11.1
6	30	14.10	100	0	16.42	0.86	100	4.52	24.0
7		19.47	100	30	16.17	1.20	740	5.02	19.3
8		21.83	100	43	16.00	1.36	253	2.45	8.4

959

960

961  
962Table 7: CO<sub>2</sub> hydrate formation and dissociation results in a sandy matrix with several particle size classes

<b>Run</b>	<b>Water Saturation S<sub>w</sub> (%)</b>	<b>Particle size class</b>	<b>Induction time (min)</b>	<b>Mass of hydrate formed (g)</b>	<b>Water to hydrate conversion rate (%)</b>
<b>1</b>	53.4	PS01	87	4.47	32.3
<b>2</b>	51.5	PS02	83	3.60	28.7
<b>3</b>	51.8	PS03	92	3.16	25.7
<b>4</b>	52.0	Non-sieved sand	52	3.39	28.1

963  
964

Journal Pre-proofs

965 Table 8: Operating conditions and results obtained from the experiments of CO<sub>2</sub> hydrate  
 966 formation and dissociation in silica gel

Run	Pore size (nm)	Mass of water injected (g)	Pore volume $S_{wp}$ (%)	Interstitial space $S_{wi}$ (%)	Induction time (min)	Mass of hydrate formed (g)	Water to hydrate conversion rate (%)
1	100	5.93	53	0	No hydrate		
2		9.01	78	0	165	4.63	38.4
3		11.35	100	0	203	4.70	30.9
4		11.01	100	0	102	4.83	32.8
5		17.98	100	32	82	2.68	11.1
6	30	14.10	100	0	100	4.52	24.0
7		19.47	100	30	740	5.02	19.3
8		21.83	100	43	253	2.45	8.4

967

968

### 969 CRediT authorship contribution statement

970 **Fatima Doria Benmesbah:** Methodology, Software, Investigation, Data curation, Writing –  
 971 original draft, Visualization. **Pascal Clain:** Supervision, Validation, Visualization, Writing -  
 972 review & editing. **Olivia Fandino:** Supervision. **Veronique Osswald:** Validation,  
 973 Visualization. **Laurence Fournaison:** Supervision, **Christophe Dicharry:** Resources,  
 974 Methodology, Writing - review & editing. **Livio Ruffine:** Project administration, Resources,  
 975 Supervision, Validation, Writing - review & editing. **Anthony Delahaye:** Project  
 976 administration, Supervision, Validation, Visualization, Writing - review & editing.

977

978

### 979 Declaration of interests

980

981  The authors declare that they have no known competing financial interests or personal  
 982 relationships that could have appeared to influence the work reported in this paper.

983

984  The authors declare the following financial interests/personal relationships which may be  
 985 considered as potential competing interests:

986

987

988

989

990

991

992

Journal Pre-proofs